D. Hooijmeijer

Dutch Aircraft Noise Model Analysis

Classification comparison with measurements

Dutch Aircraft Noise Model Analysis

Classification comparison with measurements

By

D. Hooijmeijer

in partial fulfilment of the requirements for the degree of

Master of Science
in Aerospace Engineering

at the Delft University of Technology,
to be defended publicly on Friday July 12, 2019 at 10:00 AM.

Supervisor TU Delft:	Dr.ir. M. Snellen
Supervisor LVNL:	F. Dijkstra
Supervisor AAS:	Ir. W. Dalmeijer
Thesis committee:	Dr.ir. M. Snellen
	Prof.dr. D.G. Simons
	F. Dijkstra
	Ir. J.A. Melkert

TU Delft

Abstract

Since the start of aircraft noise modelling in the Netherlands, the national noise model guidelines are prescribed in ‘het Nederlands Rekenvoorschrift’. However, as the modelling of aircraft noise is losing support, there is an increasing ask for measurement of noise. This lack of support is the main reason for KDC Schiphol (LVNL/AAS/KLM) to set up a new line of research in cooperation with TU Delft into aircraft noise calculation and measurement.

This research analyses the Dutch aircraft noise model by comparing it with measurements. More specifically, the focus is on analysing the aircraft classification as prescribed by the model by comparing single flight calculations with measurements taken by the Schiphol Noise Measurement System (NOMOS) based on the Sound Exposure Levels (SEL). The classification bundles comparable aircraft together in a group represented by flight and noise characteristics of a single representative aircraft. The largest class, accountable for approximately 50% of the flights at Schiphol, currently represents 13 aircraft types, varying from the Airbus A320 series to the Boeing 737-900, by the B737-300. Even though this classification forms the core of the model, a thorough research into its validity has never been performed.

While the original model guidelines prescribe the use of theoretical average ground tracks and distributions, reality shows that these ground tracks can differ significantly for each flight. For this reason, it is chosen to exclude this effect on the calculations and use real ground tracks for each flight. To model real flight tracks, provided by Air Traffic Control the Netherlands (LVNL), and compare the model with NOMOS measurements, provided by Amsterdam Airport Schiphol (AAS), a fit-for-purpose implementation of the Dutch aircraft noise model is created. This model is validated with an older version of the original model set up by S. Galis (NLR/LVNL).

Using this new model implementation, analysis on this class showed that, even though the total class can show good results overall, individual types within this class can show significant differences between calculations and measurements on a single event level. Further investigation shows that this is primarily related to the basic height and thrust profiles that are used for all aircraft in this class, which can deviate significantly from reality for each type specific. Correcting for these deviations in flight height and thrust setting for each type can reduce the type-specific errors and brings calculations closer to the measurements.

After the corrections, an underestimation of the noise levels remains for all aircraft types in the class. A plausible reason for this is that all used aircraft types differ from the representative aircraft in both weight and engine type, while the noise data of a single aircraft is used. To investigate this in more detail, it is recommended to have more information about real take-off weight and take-off procedure. Further recommendations include corrections for weather corrections to make the model more generally applicable and data improvement in terms of sampling rate (resolution) for both NOMOS data and flight data to reduce data-induced errors.

Acknowledgements

This MSc thesis research brought me in a very interesting and challenging way to the end of my studies. I want to thank all who have supported me throughout this process.

First of all, I want to thank the section Aircraft Noise and Climate Effects (ANCE) and Knowledge Development Centre (KDC) Schiphol for the opportunity to do my thesis externally while still remain closely connected to the TU Delft. This opportunity not only gave me the chance to develop myself scientifically, but also develop my personal and practical way of thinking in a real corporate environment at Schiphol Airport. Even though it has not always been the easiest path to align all interests, I would like to thank all my supervisors who always supported my research and were always available to have critical conversations about the work.

In that light, I first want to thank Mirjam Snellen for the support, time and feedback throughout the entire thesis. Her help in scoping my research and bringing it all back from a 'stamp collection' to a structured result really helped me in shaping the thesis.

Furthermore, I would like to thank Ferdinand Dijkstra, my supervisor for LVNL and the KDC, for all his enthusiasm and effort he put in supporting me right from the start with shaping the research question and data acquisition. The amount of time and effort Ferdinand puts in being available for students and helping them cannot be mentioned enough.

The other part of my study was conducted at Schiphol Group (AAS), where Wouter Dalmeijer has been my supervisor during the entire thesis. Wouter really helped with putting the assignment in a practical perspective and put a lot of time in reflecting the research with respect to the daily challenges Schiphol faces. The weekly meetings at Schiphol gave the opportunity to discuss all matters related to aircraft noise with the Corporate Development team and Robert Koster, also MSc thesis student at ANCE. I want to thank Robert for all the brainstorming sessions, discussions regarding noise models and personal talks we had during this period.

Lastly, just as important as the aforementioned, my family, girlfriend and friends who supported me all the way through my studies. My parents have always been there to listen and help me where they could, even though the material was sometimes maybe a little hard to understand. The same holds for my girlfriend, working on her MSc thesis as well. Both working on our theses makes it easy to reflect and help each other where needed to finish our studies at the same time.

D. Hooijmeijer
Delft, July 2019

Contents

List of Tables

List of Figures

List of acronyms

ANOMS	Airport Noise Monitoring and Measurement
ARTAS	ATM Surveillance Tracker and Server
B&K	Brüel & Kjaer
BPF	Blade Passing Frequency
CDA	Continuous Decent Approach
DFT	Discrete Fourier Transform
EPN	Effective Perceived Noise
FDR	Flight Data Recorder
HWFAP	HardWall Forward Acoustic Panel
ICAO	International Civil Aviation Organization
ISA	International Standard Atmosphere
LTO	Landing and Take-off cycle
LVNL	Luchtverkeersleiding Nederland (Air Traffic Control the Netherlands)
MTOW	Maximum Take-Off Weight
NADP	Noise Abatement Departure Procedure
NASA	National Aeronautics and Space Administration
NLR	Nederlands Lucht- en Ruimtevaartcentrum
NMT	Noise Measurement Terminal
NOMOS	Noise Monitoring System
NPD	Noise-Power-Distance
NRM	Nederlands Reken Model (Dutch Aircraft Noise Model)
PSD	Power Spectral Density
PWL	Power Watt Level
RDS	Rijksdriehoekstelsel
RoC	Rate of Climb
rpm	Revolutions Per Minute
SEL	Sound Exposure Level
SPL	Sound Pressure Level
TW	Thrust-to-Weight ratio

List of symbols

Symbol	Description	Units
B	Number of (fan-)blades	[-]
c	Speed of sound	[m/s]
f	Frequency	[Hz]
f_c	Centre frequency	[Hz]
fs	Sampling frequency	[Hz]
f'	Doppler shifted frequency	[Hz]
Δf	Frequency bandwidth	[Hz]
H	Height	[m]
I	Acoustic intensity	[W/m^2]
L_A	Overall A-weighted Sound Pressure Level	[dB(A)]
ΔL_A	A-weighting correction	[dB]
$L_{A,max}$	Maximum Overall A-weighted Sound Pressure Level	[dB(A)]
$L_{A_{sample}}$	Overall A-weighted Sound Pressure Level sample	[dB(A)]
L_{den}	Day-evening-night average level	[dB(A)]
M	Mach number	[-]
n	Engine rotational speed	[rpm]
N	Number of samples	[-]
$Nfft$	Number of samples used for Fourier analysis	[-]
p_a	Ambient pressure	[Pa]
p_e	Effective pressure	[Pa]
$p_{e,0}$	Background effective pressure	[Pa]
p'	Pressure fluctuation	[Pa]
r	Radius	[m]
t	Time	[s]
t_{frame}	Analysis timeframe	[s]
t_{span}	Sample timespan	[s]
T	Duration	[s]
T_a	Ambient temperature	[°C]
V_w	Wind speed	[m/s]
W	Source acoustic power	[Watt]
α	Absorption coefficient	[dB/m]
ϵ	Relative height	[-]
φ	Relative humidity	[%]

1 Introduction

The increase in flights worldwide also affects the Dutch aviation sector. With a 50% increase in passengers in 2018 compared to 10 years earlier, Amsterdam Airport Schiphol follows this same trend [1]. As the demand for flights increases, the number of flights that are allowed at Schiphol Airport reached the maximum of 500.000 by 2017, 3 years ahead of the new evaluation in 2020. This ceiling is not the only problem for the airport, as the number of flights increases, the annoyance related to an increasing noise exposure leads to more complaints and resistance to possible extensions above these 500.000 flights. Examples are the numerous articles and news items that are criticizing the current operations and the calculated noise estimations used for yearly communication of expected noise.

Because of this criticism and mistrust in the calculations and noise models, the demand for using noise measurements together with the models, instead of purely modelling noise, increases. This is also stressed by the new action plan for community noise by the Dutch minister of Infrastructure and Environment [2]. Even though Schiphol has a large noise measurement, Schiphol Noise Monitoring System (NOMOS), available for use, it is currently only used for illustrative means. However, there is a lot of information hidden in this system that allows for detailed assessment of noise, comparison with models and communication of noise levels.

With the introduction of the Advisory Board for Aviation Noise Annoyance in 1961, chaired by C.W. Kosten, the first step was taken towards Dutch aircraft annoyance regulation. Several years later, in 1967, the first results of the studies by the board, related to aircraft noise, were published which formed the basis for a national noise model prescribed in 'het Nederlands Rekenvoorschrift' (NRM) [3]. In that time, some questionable assumptions were made that have not yet been validated in detail. These assumptions were initially used for reducing the calculation load of the model in case of yearly estimations. As the core of the model has not changed significantly since then, these assumptions are still present in the model guidelines. An important assumption is that various aircraft can be represented by a single 'representative' aircraft. As such classes of aircraft are created, all aircraft in such a class are treated equal. However, with the introduction of new aircraft, being represented by older aircraft, the question is if the classification still holds for the current fleet.

To deal with the questions for measurement and model validation, this research will focus on comparing the NRM noise model with the measurements taken by the NOMOS measurement system.

The aim of this research is to analyze the NRM classification
by
comparing the calculated aircraft noise with measurements taken by the NOMOS measurement system.

For this research, NOMOS measurements are not only used, in the conventional way, i.e. to compare modelled and measured noise levels, but they are also used to extract more information about the flight to validate and correct the input parameters to the model. For example, by performing a spectral analysis on the sampled noise data, the thrust setting corresponding to the flight can be derived which is used as input to the model.

The latter is important, since the quality of the noise predictions is not only dependent on the model itself, but also on the quality of the input parameters. This thesis research addresses that. First, best guesses for the model input, i.e. thrust setting and height profile, are derived from reality. Only after these inputs reflect the annual situation optimally, the validity of the assumptions made in the model are investigated.

Analysis and used metrics

In this research, the calculated and measured noise events are compared based on their Sound Exposure Levels (SEL), as is shown graphically in Figure 1.1.

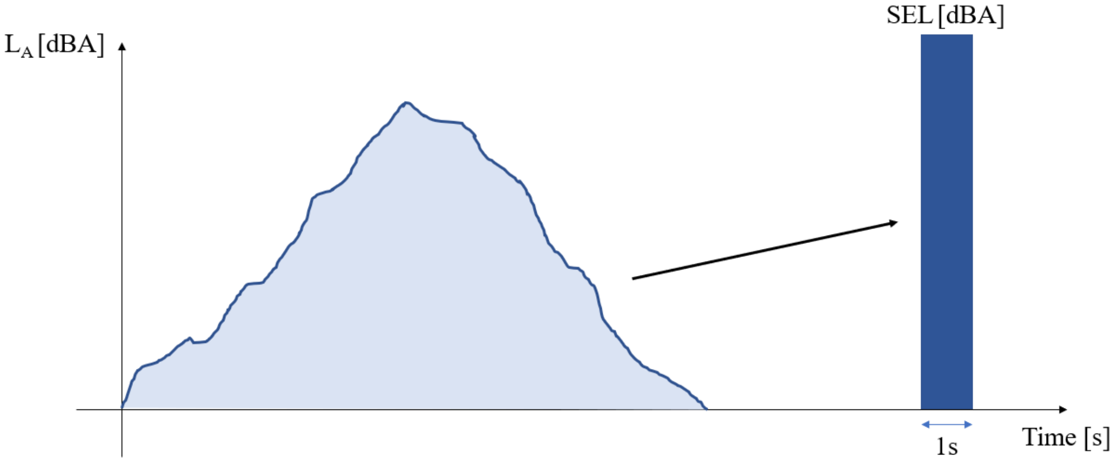

Figure 1.1. Typical Aircraft flyover noise event and corresponding Sound Exposure Level (SEL)

The SEL, in dB(A), accounts for both the event duration (T), in seconds, and corresponding instantaneous Overall A-Weighted Sound Pressure Levels ($L_A(t)$) in one metric following Equation (1.1).

$$SEL = 10 \log_{10}\left(\frac{1}{T_0}\int_{t_0}^{t_0+T} 10^{\frac{L_A(t)}{10}} dt\right) \tag{1.1}$$

The constant T_0 is for the SEL 1 second, to get a 1 second equivalent Sound Exposure Level. The integration time T is for this research based on the 10dB downtime, i.e. only time-series with a noise level down to 10dB from the maximum noise level are included. $L_A(t)$, in dB(A), is a function of the Sound Pressure Level (SPL), in dB, in the center frequency (f_c) of each frequency band corrected by the A-weighting, $L_A(f_{c,i})$ (Equation (1.2)).

$$L_A = 10 \log_{10}\left(\sum_{f_c} 10^{\frac{SPL(f_{c,i})+\Delta L_A(f_{c,i})}{10}}\right) \tag{1.2}$$

The A-weighting is a function of the centre frequency (f_c) of each band, following the 40 phon equal loudness contour (Equation (1.3)).

$$\Delta L_A(f_c) = -145 + 98{,}262 \log_{10}(f_c) - 19{,}509 \log_{10}(f_c)^2 + 0{,}975 \log_{10}(f_c)^3 \tag{1.3}$$

The SPL in each band follows from the effective pressure of the signal over time (p_e), in units Pa, compared to the background reference pressure ($p_{e,0}$), equal to 2*10^{-5} Pa (Equation (1.4)).

$$SPL = 10 \log_{10}\left(\frac{p_e^2}{p_{e,0}^2}\right) \tag{1.4}$$

This process is explained in more detail in Chapter 4.2.

Strengths and weaknesses of SEL

As already mentioned, the strength of the SEL is that it captures both the duration and noise level time series in one metric. In this way, all events can be compared by a single metric capturing the complete event. It is able to give a more complete representation of the event compared to the original metric, the Maximum Instantaneous A-weighted Sound Pressure Level ($L_{A,max}$), which only indicates the maximum noise level and does not include the duration of the event.

However, there are also pitfalls to this metric. As it is now a function of time and noise level, a long event with low noise can be assumed equal to a short event with a high peak noise level. In this way, it does not provide information about the noise event shape.

Using the Sound Exposure Level as metric gives more freedom in the design of flight routes and procedures compared to L_{Amax}. An example of this is the new NADP2 flight procedure, which favors a horizontal speed increase over a climb for areas close to the airport. In this way, the duration of the noise event is shorter, as a result of the higher ground speed. However, it leads to a higher peak noise level due to the lower flight height. Combining both in a single metric gives the possibility to optimize the height-speed trade-off for minimum Sound Exposure Level.

2
Methodology

2.1. Research Outline

This research aims at analysing the Dutch noise calculation model by comparing the modelled noise levels with measurements taken by the NOMOS measurement system. The reason for this research is the growing demand for validating noise models with real measurements to bring the models closer to reality. Next to this, the Dutch noise model makes use of specific assumptions like classification of aircraft while the effect of this is never researched in detail. Combining both interests, the aim of this research is to analyse the effect of the classification on the noise model performance by comparing the model calculations with measurements.

The focus of this research is on the largest present class at Schiphol Airport, class 4/3, indicated by '469' in the classification. This class represents approximately 50% of the total number of flights at Schiphol Airport. To use the model only for its prescribed conditions, the available flights are filtered using a meteo-window. In this way, only flights that occur during a certain range of meteorological conditions are analysed. This range is such that all other flights are excluded from this research as corrections for weather conditions are requested that are not implemented in the original guidelines. The original guidelines only allow for yearly calculations when assuming year-round average conditions.

For this research, as a first step, the noise model is implemented in MATLAB. This gives the possibility to adjust model parameters and calculations without having to change the available (web-)implementations of the model. Furthermore, the existing implementations have only limited possibilities in terms of replacing the theoretical input data by real data, like real flight tracks. For these reasons, a fit for purpose model is developed that is capable of doing calculations using individual track-data and implementing measurements. First, the model is validated with an existing implementation based on the same guidelines. After that, the model is used to directly compare calculations to corresponding measurements on single event and multi-event scale. Any differences occurring as a result of deviations in track height and thrust setting are assessed and discussed. Subsequently, these deviations are corrected for by implementing the real track height and thrust setting for each flight and aircraft type respectively. This step eliminates model-data deviations induced by the input parameters deviating from their actual values.

2.2. Research Design and model setup and validation

The model that is used for this research is based on the guidelines as prescribed in 'het Nederlands Rekenvoorschrift' [4]. The modelling core is supplemented by appendices that prescribe the input data to the model [5]. As already mentioned, a new implementation in MATLAB is established as part of this study. The available (web)-implementations of the model did not provide any insight in the modelling core of the model, did not allow for calculations with real data or were based on an older version of the guidelines. For this reason, a new fit for purpose implementation was requested.

The appendices that are linked to this model, consisting of input information and read-off tables, have been updated in 2014 [5]. Compared to the existing models, this new implementation is designed for calculations with both theoretical and real flight data. It has the possibility to implement the real flight track for each analysed flight individually. Next to this, it is also capable of changing the theoretical thrust setting to a measured thrust setting for each aircraft type.

The model is validated with the implementation by S. Galis (NLR/LVNL). Even though Galis' implementation is based on an older version of the appendices, the same model guidelines are used. For this reason, the validation is performed using an older flight profile that is implemented in both models. The validation is done in three steps. First, the noise contours are compared by visual inspection to identify any large modelling errors. As this is not the case, the SELs are calculated in an equal grid for both models and assessed by the relative error in each grid-point. However, this relative error does not indicate the absolute size of the errors that occur. To account for the absolute errors in the validation, the calculated SELs by the new implementation are for each grid-point compared individually against the results by Galis in a scatter plot.

2.3. Data collection

The study uses flight data and noise measurements taken by measurement stations on the ground. This data is not publicly available and is for this research provided by the owners of the data. Because of this, the data is made available for this specific use only and cannot be shared freely.

The flight data is provided by Air Traffic Control the Netherlands (LVNL). This flight data is coming from the ARTAS system at LVNL, which combines and processes the radar-data from the radar-systems on site [6]. The radar-data is managed by LVNL and used for research and performance analysis. As the radar-data is used by the air traffic controllers to guide the aircraft through the crowded airspace around Schiphol Airport, a high-level of accuracy is required.

The measured noise data comes from the Schiphol Noise Monitoring System (NOMOS) by Brüel and Kjaer. This data is managed by Amsterdam Airport Schiphol and is used for illustrative and communicative purposes. The real-time measurements and general information are shared on the Casper NOMOS website which is openly available [7]. For this thesis research, the detailed information and individual flight data is used for performance analysis and for answering specific questions from the community regarding noise annoyance.

2.4. Result analysis

The flights are analysed by comparing the calculated SEL to the corresponding measured SEL for each event individually. In the first step, the model is used to compare complete modelled noise events to the corresponding measured noise events. In this step, a detailed assessment is done to evaluate differences identified in the time-series and how they work their way through to the SEL. This shows how the model performs compared to reality on a small scale.

In the next step, the calculated and measured SELs are compared on a larger scale for all selected flights for theoretical input data. The results are shown in a scatter plot in which the measured SELs are plotted against corresponding calculated SEL. To analyse the differences per aircraft type, the average errors between measurement and calculation are plotted for each type at each NOMOS Measurement Terminal (NMT). Based on the type-specific results, the performance of the classification resulting from the theoretical class input data is assessed.

After this, the effect of differences between theoretical and real input data are investigated. In this part, the theoretical class input data is compared to real data for both track height and thrust setting for each type specifically. As a result, the theoretical inputs are replaced by real data to match the model input as good as possible with reality. In this way, the differences resulting from model input errors are minimalized and statements about the modelling core can be made.

3

Model Setup and Validation

This chapter gives an overview of the Dutch NRM model that is implemented and used in this research. The model is based on the aforementioned Dutch calculation guidelines. First, the model setup will be described in detail in Chapter 3.1, elaborating on the inputs, calculation algorithms, outputs and changes with respect to the guidelines. Subsequently, in Chapter 3.2, the model is implemented in MATLAB and validated with the older NRM implementation by S. Galis.

3.1. Model Setup

The guidelines in NRM prescribe how to model aircraft noise at Schiphol Airport. To simplify the model calculations, tables are used as input given in the appendices [5]. This set of input tables consists of 3 groups:

- Classification of aircraft types into classes
- Flight profiles for each class
- Noise data for each class

All three inputs are discussed in this chapter.

3.1.1. Aircraft classification

As input to the model, aircraft classes are specified that represent multiple aircraft types with comparable weight and noise characteristics. The aircraft are subdivided into 9 weight categories based on their Maximum Take-Off Weight ($MTOW$) as shown in Table 3.1. To exclude small, mostly propeller driven traffic from the calculations, a threshold has been set at 6000 kg MTOW.

Table 3.1. Weight categories used for the NRM aircraft classification

Weight category	MTOW (x1.000 kg)
1	$6 \leq MTOW < 15$
2	$15 \leq MTOW < 40$
3	$40 \leq MTOW < 60$
4	$60 \leq MTOW < 100$
5	$100 \leq MTOW < 160$
6	$160 \leq MTOW < 230$
7	$230 \leq MTOW < 300$
8	$300 \leq MTOW < 400$
9	$MTOW \geq 400$

Since only including weight does not account for technological progress in aircraft design, each weight category is linked to 4 noise categories based on the aircraft certified noise levels. These certified noise levels are measured during the certification flight and corrected for atmospheric conditions, following the procedure prescribed by ICAO [8]. The ICAO certification measurement setup for the complete landing- and take-off (LTO) cycle is shown in Figure 3.1. For expressing the certification measurements, use is made of the Effective

Perceived Noise Level ($EPNL$). This metric expresses the relative noisiness of an aircraft noise event, in Effective Perceived Noise Decibels ($EPNdB$), and is a combination of maximum noise level, duration and tone.

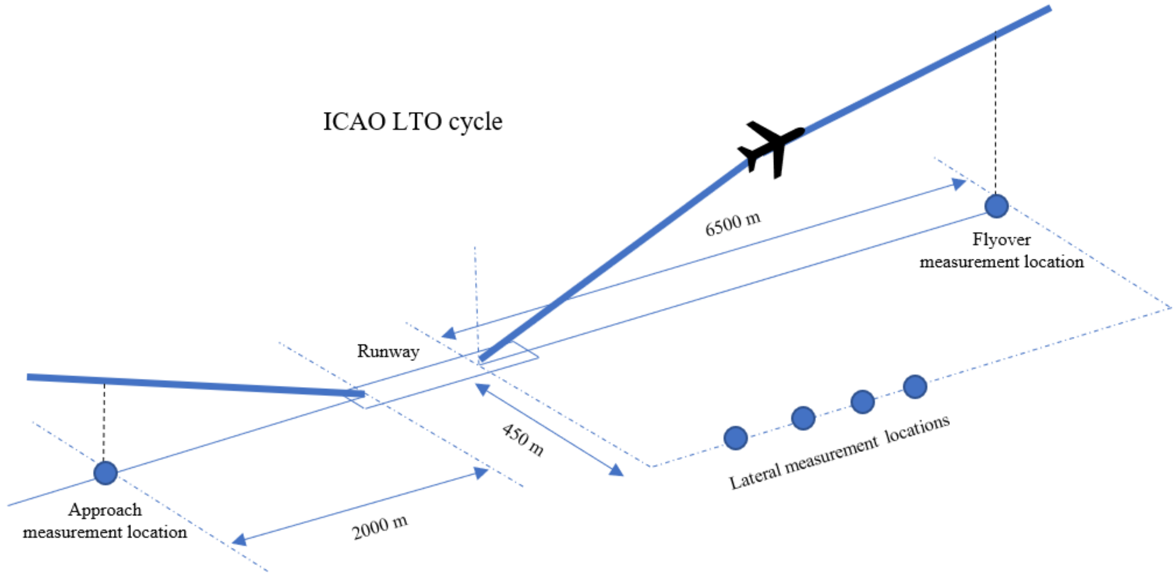

Figure 3.1. ICAO certification measurement setup for a complete LTO cycle

The sum of the measurements taken at all measurement locations, in $EPNdB$, is used to assign an aircraft to a noise class. The sum of the certification measurements ($\sum_{type} EPNdB$) of an aircraft in a weight class is compared to the limiting, representative aircraft of this weight class ($\sum_{limiting\ type} EPNdB$). The difference in certified noise level determines the noise class of the aircraft ($\Delta EPNdB$).

$$\Delta EPNdB = \sum_{type} EPNdB - \sum_{limiting\ type} EPNdB \tag{3.1}$$

Since the noise levels for new aircraft types are generally lower than the limiting aircraft type within the same weight class, the resulting values for $\Delta EPNdB$ are negative. In case of a non-negative value, the aircraft type will automatically be assigned to noise class 1 as is shown in Table 3.2.

Table 3.2. Noise classes used for the NRM classification

Noise class	$\Delta EPNdB$
1	$\Delta EPNdB > 0$
2	$0 \geq \Delta EPNdB > -9$
3	$-9 \geq \Delta EPNdB > -18$
4	$\Delta EPNdB \leq -18$

Combining the 9 weight categories with the 4 noise classes, 36 aircraft classes are set up, each having one representative aircraft or using a representative aircraft of another noise class with a correction of several dB. This table of representative aircraft has been specified by NLR and is part of the appendices that are used for the Dutch aircraft noise model [5]. A complete overview of the classes and representative aircraft is shown in Table 3.3.

Table 3.3. Overview of the NRM classification and representative aircraft for each class

Weight category	Noise class 1	Noise class 2	Noise class 3	Noise class 4
1	BAe-3100 Jetstream 31	BAe-3100 Jetstream 31	BAe-3100 Jetstream 31	BAe-3100 Jetstream 31
2	Fokker F-28 Fellowship	Fokker F-27 Friendship	Fokker 100	Fokker 70
3	Boeing 737-200	DC-90-30 (-3 dB)	Boeing 737-300 HWFAP	BAe-146-200
4	Boeing 737-200	Boeing 737-300	Boeing 737-300 HWFAP	MD-90
5	DC-8-63	Airbus A-310-203 (+3 dB)	Airbus A-310-203	Boeing 757-200/ RB211-535E4
6	DC-8-63	Boeing 767-300 ER (+3 dB)	Boeing 767-300 ER	Boeing 787-8
7	DC-10-30 (+3 dB)	DC-10-30	DC-10-30 (-3 dB)	Boeing 777-200
8	Boeing 747-200B	Boeing 747-300	Boeing 747-400	Boeing 777-300ER
9	-	-	-	Airbus A380-861

The full list including all aircraft types landing and departing from Schiphol Airport is also available in the appendices. Each aircraft type is assigned to one category and is in this way represented by the representative aircraft and its characteristics. The dominant category 4/3 (469) which accounts for most of the flights on Schiphol, is shown in Table 3.4. As is shown, most of the operational 737s and A320s are placed in this class.

Table 3.4. Nederlands Rekenvoorschrift aircraft class 4/3 (469) represented by Boeing 737-300

ICAO code	Full name
A306	Airbus A-300B4-600
A319	Airbus A-319, ACJ
A320	Airbus A-320
A321	Airbus A-321
B734	Boeing 737-400 for companies KLM/KLC/TRA/MPH/AHR
B736	Boeing 737-600
B737	Boeing 737-700, BBJ
B738	Boeing 737-800, BBJ2
B739	Boeing 737-900
MD81	MCDonnell Douglas MD-81
MD82	MCDonnell Douglas MD-82
MD87	MCDonnell Douglas MD-87
MD88	MCDonnell Douglass MD-88

All these aircraft types are represented by the same 737-300, using the HardWall Forward Acoustic Panel acoustic engine modification (HWFAP) [9]. Because of this representation, noise characteristics are assumed independent of the actual configuration and engine type.

3.1.2. Flight profile

For each aircraft class, flight profiles and noise-power-distance (NPD) tables have been constructed. When the aircraft class has been set, the flight profile is selected based on the procedure and the distance of the flight. This profile gives a complete set of height versus distance, flight speed and corresponding thrust settings for a general take-off procedure. Since these profiles are determined for ideal situations, the real flight profile will in most cases deviate from this, for example because of human input, (engine) transients, vertical uncertainties and aircraft configurations.

The flight procedures have been split into 3 categories: start, landing and circuits. The start category consists of 9 procedures, including standard ICAO procedures, but also airport specific procedures like derated take-off thrust or NADP (Noise Abatement Departure Procedures) as designed for noise reduction and used by several airlines. The landing category has 3 procedures, consisting of aircraft settings being: a 'normal instrument approach', a 'low power low drag approach' and a 'reduced flap approach'. Where the normal instrument approach uses the standard landing configuration, low power low drag and reduced flap approach use adjusted aircraft settings to reduce the emitted noise during landing procedures by reducing engine and airframe noise. The used take-off and landing procedures are shown in Table 3.5 and Table 3.6 respectively.

Table 3.5. Take-off procedures used in NRM

Take-off code	Procedure
00	'Other than 01-08'
01/02	Derated start
03	ICAO-B start
04	Derated start with changed flap settings
05	ICAO-A start
06	NADP2 start, climb 1.500 ft
07	NADP2 start, climb 1.000 ft
08	NADP2 start, climb 800 ft

Table 3.6. Landing procedures used in NRM

Landing code	Procedure
10	3° glide angle, normal instrument approach
11	3° glide angle, low power low drag
12	3° glide angle, reduced flap approach

Next, the class number of the flight is determined. For take-off (Table 3.7), the class number represents the distance of the flight, based on the destination. In case of landing (Table 3.8) the class number gives additional information about the landing procedure, like the initial approach height, in case of step approach, or the continuous descent approach (CDA).

Table 3.7. Class numbers NRM based on distance to destination

Take-off class-number	Distance to destination [km]
00	$D \leq 750$
01	$750 < D \leq 1.500$
02	$1.500 < D \leq 3.000$
03	$3.000 < D$

Table 3.8. Landing class numbers NRM based on additional landing information

Landing class-number	Procedure information
00	Initial approach altitude 2.000 ft
01	Initial approach altitude 3.000 ft
09	Continuous descent approach

For each procedure-class combination, flight profiles have been determined and are tabulated in the appendices. As an example, a Boeing 737-800 flying from Schiphol to Paris using an ICAO-A start procedure can be used. The ICAO code of this airplane is B738 which is listed in category 469, represented by the 737-300 HWFAP. The ICAO-A starting procedure is listed as procedure 05 and since the distance from Schiphol to Paris is under 750 km, this flight is placed in class 00. The full administration number of this flight for noise calculations will thus be: 4690500. Corresponding to this number, the flight profile table of this specific flight is shown in Figure 3.2.

```
Vliegtuigcategorie of vliegtuigtype      : 469
Klasse                                   : 0500
Representatief vliegtuig type en gewicht : B737-300; CMF56-3-B2; 52400 kg
Procedure                                : START; ICAO-A

Versie nummer                            : 2
Datum/tijd laatste modificatie           : 98-06-02 09:38:19

Hoogteprofiel:

   SEGMENT      W          H          H         T          GAM       V
               (m)        (m)        (ft)   (FAN/rpm)     (deg)    (m/s)

                0.0        0.0        0.0    4805.00
        1                                                  0.0     39.60
             1144.0        0.0        0.0    4805.00
        2                                                  6.2     79.20
             1242.0       10.7       35.0    4805.00
        3                                                  6.2     81.30
             1788.0       69.8      229.0    4806.00
        4                                                 12.0     82.80
             3614.0      457.2     1500.0    4834.00
        5                                                 11.7     83.30
             3645.0      463.6     1521.0    4704.00
        6                                                 10.1     84.90
             6170.0      914.4     3000.0    4741.00
        7                                                  2.6    111.10
            10498.0     1112.8     3651.0    4712.00
        8                                                  8.2    137.90
            17543.0     2133.6     7000.0    4791.00
```

Figure 3.2. Flight profile table for flightnumber 4690500

The data in Figure 3.2 is used to reconstruct the flight path and corresponding thrust settings for each segment of the path. Height profile and thrust settings, with respect to the distance from take-off, are shown in Figure 3.3. For illustrative purposes, the thrust settings given in the profiles, in Fan/RPM are converted to a percentage by using the maximum fan rotational speed.

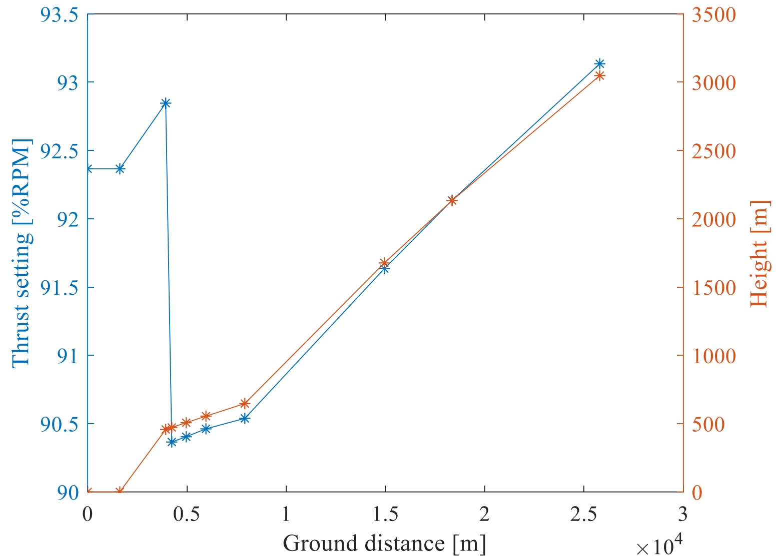

Figure 3.3. Height profile and thrust setting for ground distance (flightnumber 4690500)

From Figure 3.3, it is found that for an ICAO start the thrust setting remains within a small margin of several percent of the take-off thrust. In this figure, transients are not shown, since this would require more information of the transient behaviour of the engine. For this reason, a linear change of thrust is assumed. To use this data in a temporal domain, which is needed to calculate temporal metrics like the day-evening-night average level (L_{den}), a conversion from distance to time is performed. This conversion makes use of the segment (ground-) velocity that is reported in the last column of the profile table.

The thrust setting is used together with the aircraft-observer distance to calculate the sound exposure at the observer's position as a result of the flyover based on the Noise-Power-Distance-tables (NPD).

3.1.3. NPD data

The noise data corresponding to this category is listed in a table consisting of the noise levels in dB(A) for pre-determined source-receiver distances and engine settings. The engine settings for which the noise levels are tabulated are either a thrust index, thrust force (kN) or fan rotational speed (rpm). For class 469, the fan rotational speed is used which follows from the fan speed percentage, in Figure 3.3, multiplied with the maximum fan rotational speed for that engine. The NPD table for class 469 is shown in Figure 3.4, where this rotational speed is used to find the noise value for pre-set distances.

3.28 Categorie 469

```
Vliegtuigcategorie of vliegtuigtype : 469
Representatief vliegtuig type       : B737-300/400 ; CFM56-3 HWFAP
Afscherming                         : wel
Versie nummer                       : 2
Datum/tijd laatste modificatie      : 98-06-02 09:38:19
```

Geluidsniveau's (dB(A)):

log s	s (m)	2325.00	2825.00	3450.00	3580.00	3760.00	3940.00	4480.00	5200.00
		THRUST (FAN/rpm)							
1.78504	61.0	90.45	93.02	97.38	96.50	96.88	97.43	100.15	106.25
2.08607	121.9	83.46	85.80	90.14	89.81	90.24	90.84	93.57	99.44
2.26217	182.9	79.34	81.51	85.86	85.75	86.24	86.87	89.61	95.25
2.48401	304.8	74.03	75.98	80.37	80.43	80.98	81.66	84.40	89.75
2.78504	609.6	66.26	68.08	72.61	72.67	73.31	74.05	76.82	81.83
3.08607	1219.2	57.49	59.30	64.06	64.04	64.73	65.51	68.38	73.41
3.26217	1828.8	51.62	53.59	58.47	58.36	59.07	59.87	62.86	68.22
3.38710	2438.4	46.93	49.15	54.07	53.95	54.65	55.47	58.61	64.39
3.48401	3048.0	42.99	45.48	50.39	50.27	50.98	51.82	55.10	61.29

Figure 3.4. Noise-Power-Distance table NRM category 469

Noise levels corresponding to other distances are calculated by linear interpolation between the logarithm of the distance and the thrust setting. By using a semilog plot, more or less linear behaviour is found where small non-linearities are the result of absorption losses.

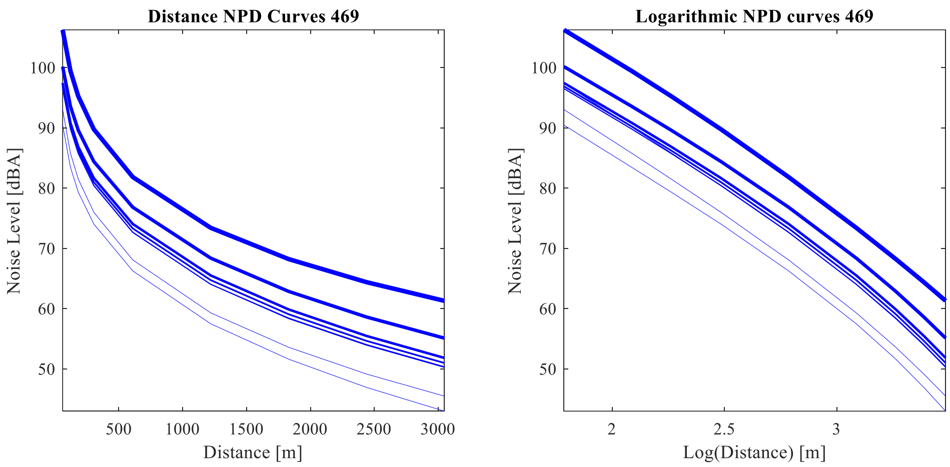

Figure 3.5. Standard (left) and semilog (right) plot NPD curves

NRM does not include any directivity effects in noise emissions. Because of this, the aircraft are represented as an omnidirectional point source emitting sound waves in all directions equally, as is shown graphically in Figure 3.6. Assuming conservation of energy, without absorption losses, the spherical spreading of the sound reduces the sound intensity on the surface with the increasing distance from the source (radius). As the surface of the sphere increases by the radius squared, the intensity decreases following the relation in Equation (3.2).

$$I = \frac{W}{4\pi r^2} \tag{3.2}$$

In this relation, I is the acoustic intensity on the surface (W/m^2), W is the point source acoustic power (Watt) and $4\pi r^2$ is the area of the surface of the sphere, from the radius (r). The r^2 term leads to the behaviour as shown in Figure 3.5.

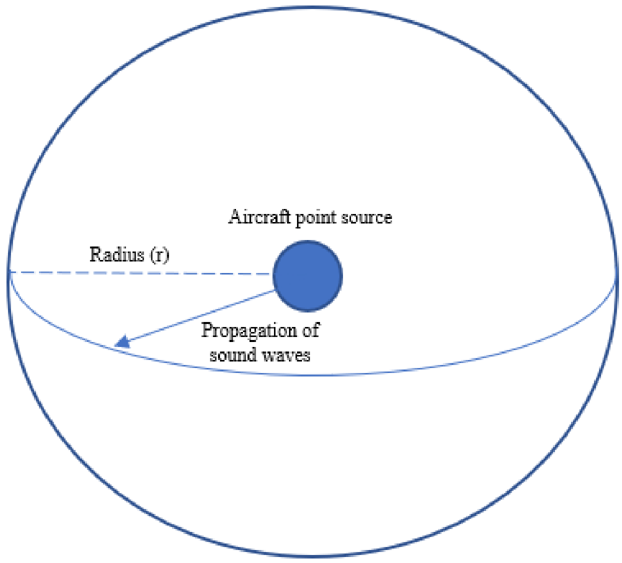

Figure 3.6 Omnidirectional emission of noise from a point source

This can also be converted to acoustical terms using the sound pressure level at a distance from the source and the source power watt level as is derived in [10]:

$$SPL(r) = PWL - 10.8 - 20\log(r) \tag{3.3}$$

In Equation (3.3), PWL denotates the source Power Watt Level and SPL is the Sound Pressure Level at a distance r from the source. If this is relation is applied to the above noise tables to derive the source PWL, a non-constant value is found (Figure 3.7).

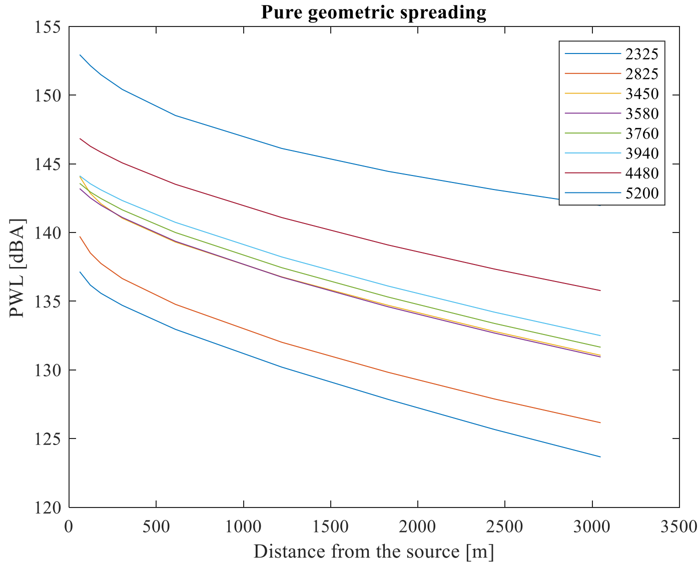

Figure 3.7. Source PWL calculated from NPD tables using spherical spreading

The change in calculated PWL indicates that there are also propagation effects other than geometrical spreading included in the tables. Assuming that these propagation effects only consist of absorption and increase linearly with the radius [10], an absorption coefficient is introduced.

$$PWL = SPL + 10.8 + 20\log(r) + \alpha r \tag{3.4}$$

With the distance ‘r’ and the corresponding Sound Pressure Level being known, the absorption coefficient is derived by using Equation (3.4).

$$PWL(r_1) = PWL(r_2) \tag{3.5}$$

$$SPL(r_1) + 10{,}8 + 20\log(r_1) + \alpha r_1 = SPL(r_2) + 10{,}8 + 20\log(r_2) + \alpha r_2 \tag{3.6}$$

Which is rewritten to obtain the absorption coefficient between two radial distances r_1 and r_2:

$$\alpha = \frac{SPL(r_1) + 20\log(r_1) + \alpha r_1 - SPL(r_2) + 20\log(r_2) + \alpha r_2}{r_2 - r_1} \tag{3.7}$$

By applying Equation (3.7) to the NPD tables, a ‘reversed engineering’ approach, the absorption coefficient is calculated for each of the distances listed. Note that this is the full spectrum absorption, where the absorption is dependent on individual frequencies.

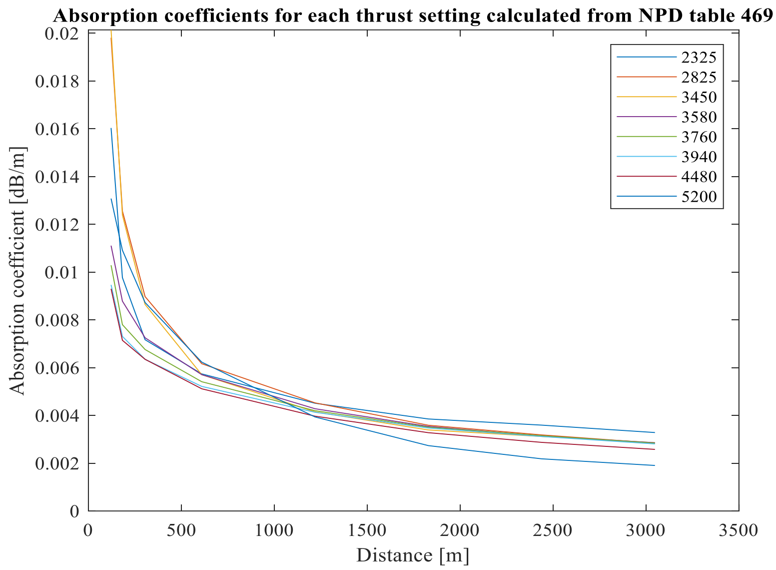

Figure 3.8. Absorption coefficients for the 469 NPD tables for varying thrust settings

The total absorption coefficients for each distance are shown in Figure 3.8 for thrust settings varying from 2325-5200 rpm. In theory, this absorption coefficient is dependent on the various frequencies that are present, and dominant, in the sound. The differences in absorption coefficient shows that there are different dominant frequencies present in the sound emitted for varying thrust settings.

3.1.4. Weather conditions

Both the NPD and Flight-profile tables have been determined for ICAO standard ISA conditions, and are because of this in a direct use only valid for these conditions. Consequently, correction factors need to be applied when deviations from these standard values occur. The weather conditions for which the tables can be used without a correction are listed in Table 3.9.

Table 3.9. ISA weather conditions (source: ICAO)

ISA conditions ICAO	
Pressure at sea level	1013 hPa
Air density	1,225 kg/m^3
Temperature	15°C
Relative humidity	70%
Wind	None
Precipitation	None

In the multi-event use of the model, these effects are expected to average out. However, for single event noise modelling, these do play a role. The effects of weather conditions on sound absorption have been investigated by NASA in 1967 [11]. In the research, it is shown that the absorption is largely dependent on the frequency. In general, an increase in frequency leads to an increase in absorption coefficient which means that high frequencies are attenuated faster (Figure 3.9).

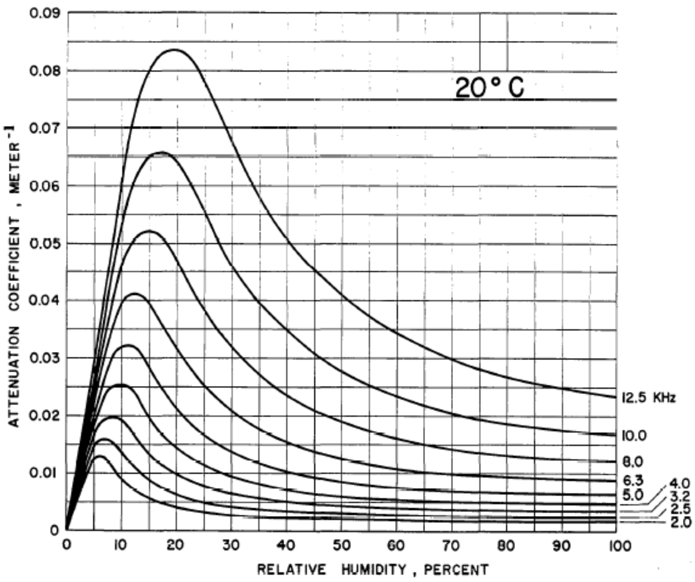

Figure 3.9. Effect of relative humidity on sound attenuation (source: NASA)

The area of interest is the relative humidity around 70%, as is prescribed in the ISA standards. For 20°C, the frequencies up to 5.000 Hz show a smaller than 5% change in absorption for the 20% interval around 70% (60-80%) relative humidity. Above 5.000 Hz, this effect increases significantly, with a change of more than 10% for the same interval of 60-80% relative humidity. Since these effects are measured for 20°C, while a temperature of 15°C is prescribed in the ISA conditions, the temperature effects should be examined as well. These effects are shown in Figure 3.10.

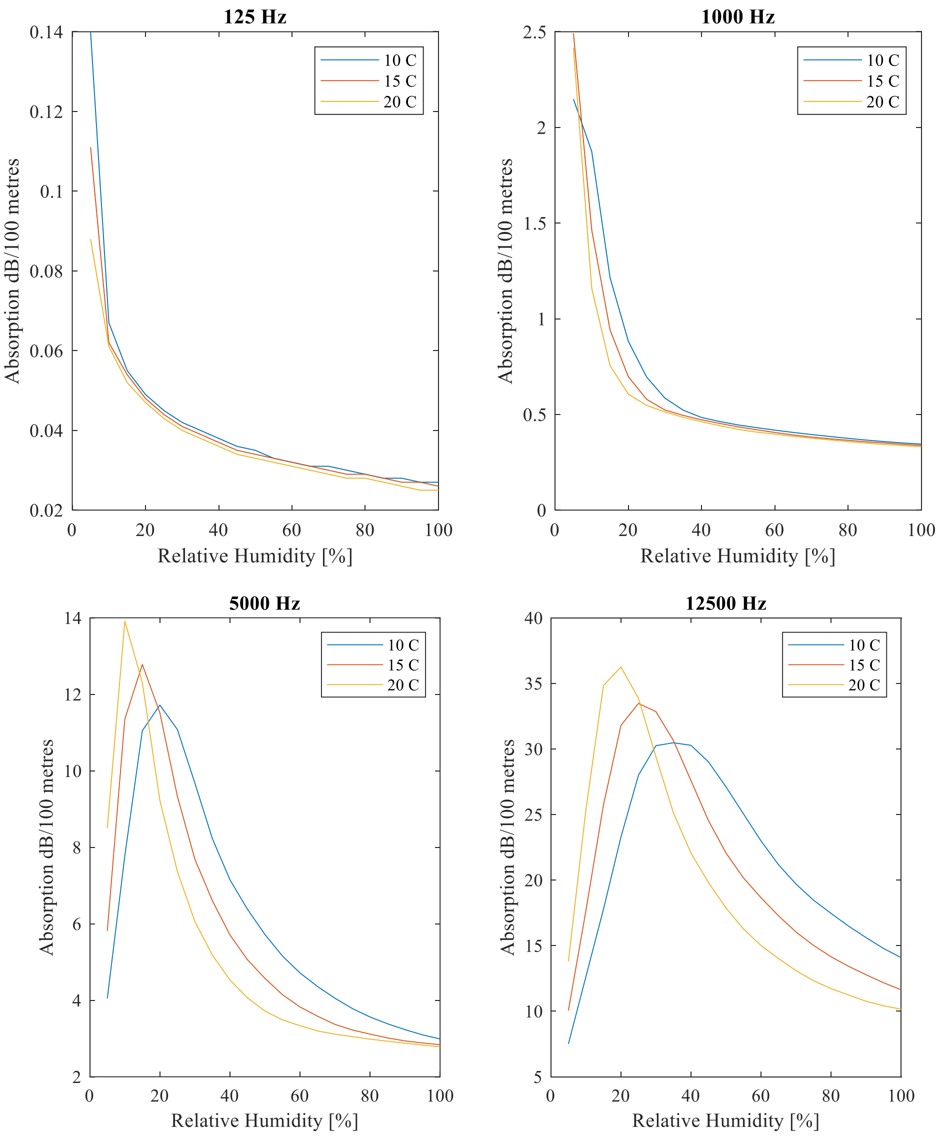

Figure 3.10. Effect of temperature on sound attenuation (source: NASA)

In Figure 3.10, it is shown that temperature effects play a minor role on the absorption for frequencies up to 1.000 Hz for all values of the relative humidity. At 5.000 Hz, the absorption values start showing deviations at low relative humidity. Increasing the frequency further also increases the deviations in the absorption-curves for different temperatures. For the prescribed relative humidity of 70%, the 125 Hz and 1000 Hz plots show that the absorption coefficients are for all temperatures on the same line. However, for 5000 Hz and 12500 Hz, the absorption coefficients at 70% relative humidity show larger differences for temperature.

This shows that for detailed modelling, frequency spectra and weather conditions should be modelled carefully. In order to use the model for single event noise calculations, the weather conditions during the flight should be close to the ISA standard conditions in case the noise spectrum contains strong high frequency components. For lower dominant frequencies, larger deviations from the ISA conditions are allowed.

3.1.5. Adjustments to the model

The model as used in this research is an adjusted version of the original model as prescribed in the guidelines [4]. These adjustments are implemented to improve the model calculations and simplify the comparison to measurements.

First, the time-step resolution is altered from 2 seconds to 1 second. The reason for this smaller timestep is that the model is originally designed for large scale multi-event simulation of a yearly traffic for which the computational time was limiting. However, for the application in this research, where a selection of single events is modelled, these calculation times are already reduced significantly. As the calculations are compared to the measurement data with a 1 second resolution, an equal resolution is now used as well for direct comparison. Furthermore, the increased resolution can be used as current computational capabilities are higher than at the time when the model was set up which reduces the computational requirements even more.

As a result of the relatively large timesteps, the original guidelines prescribe a variable timestep when approaching the transition location between two segments to follow the theoretical profile exactly. This is done to reduce the effect of the large timestep of 2 seconds that is used for calculations at discrete locations, or the even larger timestep of 10 seconds that is used for the noise contour calculation. For the new implementation, this variable timestep is left out assuming that a 1 second timestep allows for a sufficiently accurate description of the profile. By reducing the timestep to 1 second, the height deviation at transition locations is reduced to several meters, which is assumed small enough to not have a significant influence on the calculations. This is shown for one of the transition locations in Figure 3.11, showing the theoretical profile, followed exactly by the original model, and the profile resulting from the new implementation using a 1 second timestep.

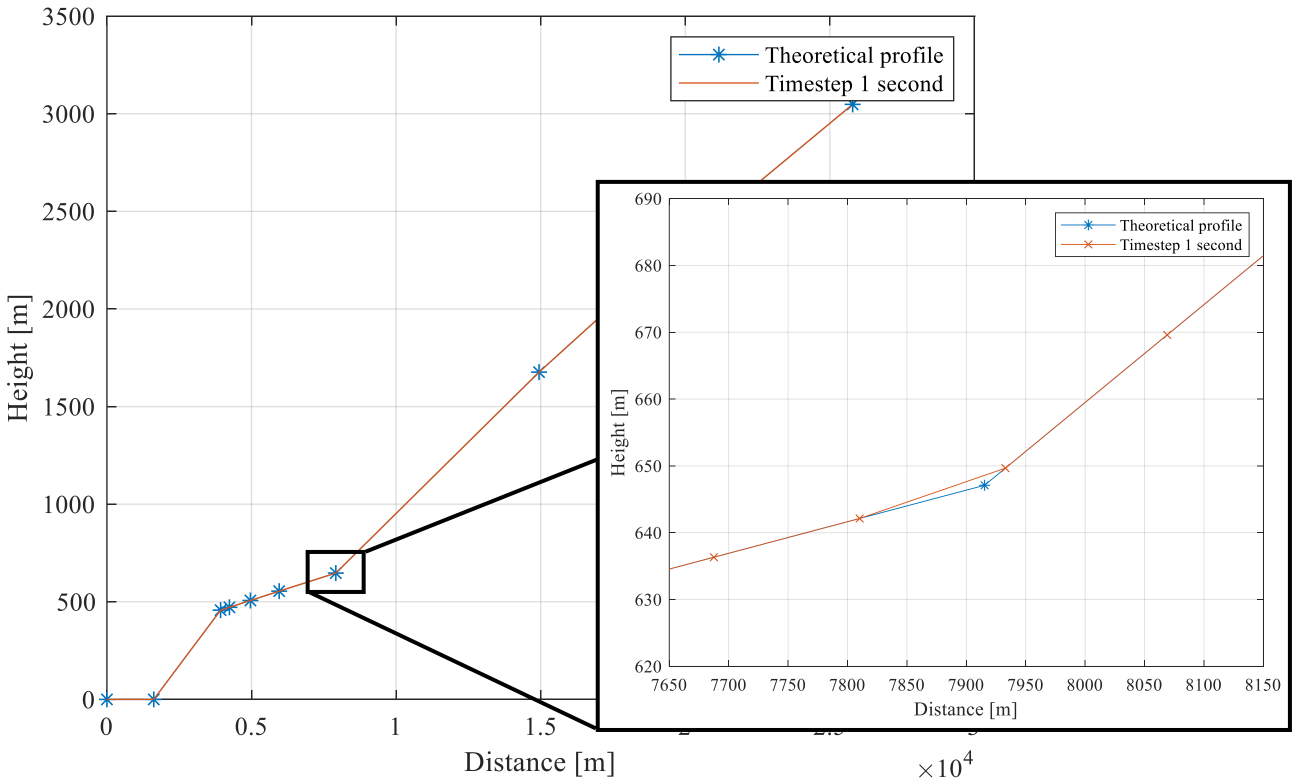

Figure 3.11. Height profile approximation using a 1 second timestep

Comparing this 1 second timestep to the results using larger timesteps as originally prescribed by the model, i.e. 2 and 10 seconds, the improvement that is achieved with respect to those timesteps on approximating the profile becomes clear. Figure 3.12 shows the deterioration in approximation that occurs when using larger timesteps.

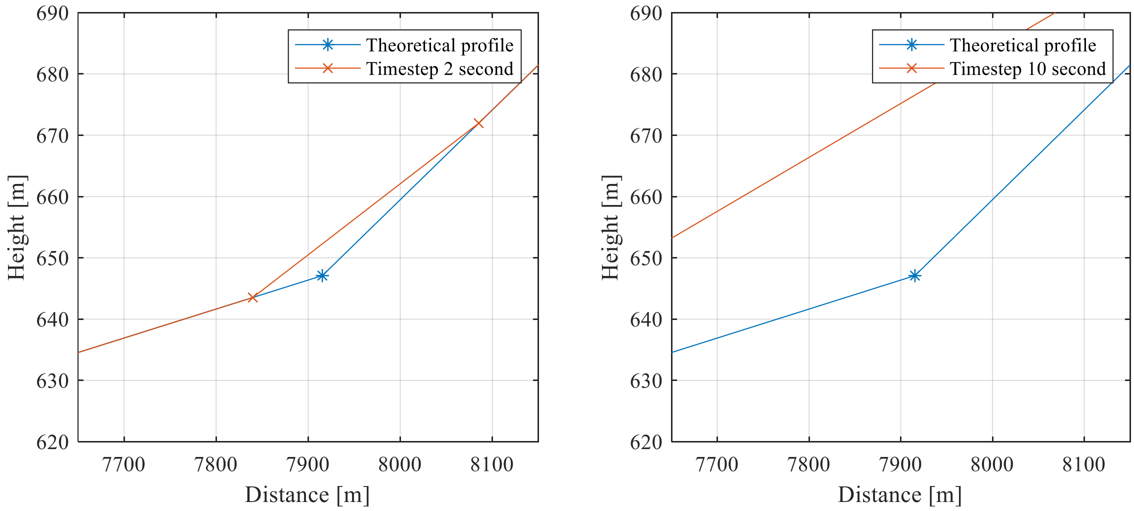

Figure 3.12. Two second (left) and ten second (right) approximation of height profiles

From Figure 3.12, it can be seen that for 2 seconds, the error still remains within the order of 10 meters, where for the timestep of 10 seconds, the error is up to several tens of meters. Another effect of the larger timestep is that this error occurs over a larger timespan, where for the timestep of 1 second, the error has a maximum duration of 1 second.

Concluding, reducing the timestep to 1 second is able to improve the resolution of the results and allows for better comparison with the measurement data. It leads to a sufficiently small resolution, up to several meters, to not further reduce the timestep at the transition location of profile segments as is originally prescribed in the model guidelines.

3.2. Model validation

The newly implemented MATLAB version of NRM is validated with an NRM implementation by Stephan Galis (NLR/LVNL). This model by S. Galis is based on the same NRM guidelines and calculates with the same input profiles and NPD-tables as are implemented in the new model that is used for this research. To validate the model, SELs are calculated in a fixed grid using both models and compared.

3.2.1. Procedure

The procedure that is used for the validation is corresponding to flight-number 4690501. An example of a flight using this procedure is a Boeing 737 (469) performing an ICAO NADP1 (05) take-off with destination Barcelona (01). This flight is graphically shown in Figure 3.13.

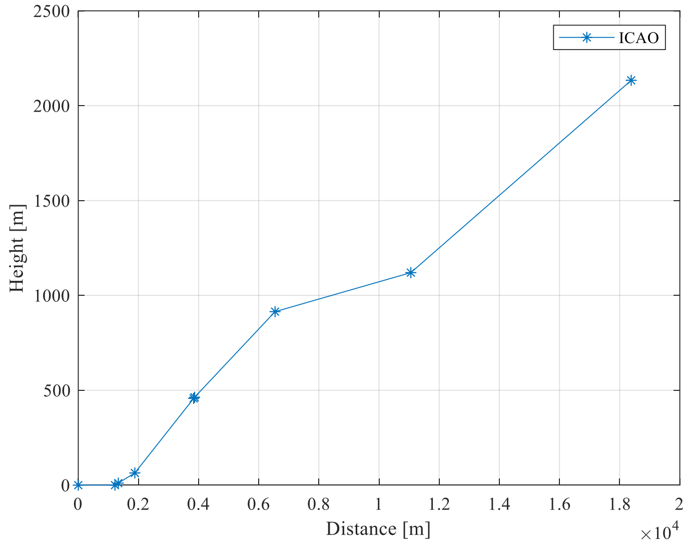

Figure 3.13. Height profile corresponding to flightnumber 4690501

Flight-number 4690501 is the newest implemented profile in the model by S. Galis. Because of this, newer (NADP2) procedures are not considered in this validation. The used 4690501 thrust- and height-profiles have been verified with the latest version of the appendices for both models [5].

To convert this to a three-dimensional track, a ground track is assigned to this height profile. For comparison, both models use a straight ground track resulting in a symmetrical sound exposure along both sides of the track. Curved flight paths are not included in this validation as the effects of curves, like the bank angle, are not included in the model guidelines and are because of this modelled in the same way as straight flight paths.

3.2.2. Grid

The noise levels are calculated in a pre-defined symmetrical grid of 4.000 m by 15.000 m, capturing the largest part of the prescribed flight profile. The grid has a 250 m grid spacing, which is finer than the usual 500 m spacing prescribed in the original guidelines to increase number of grid points for the validation. The grid is shown along with the flight track in Figure 3.14.

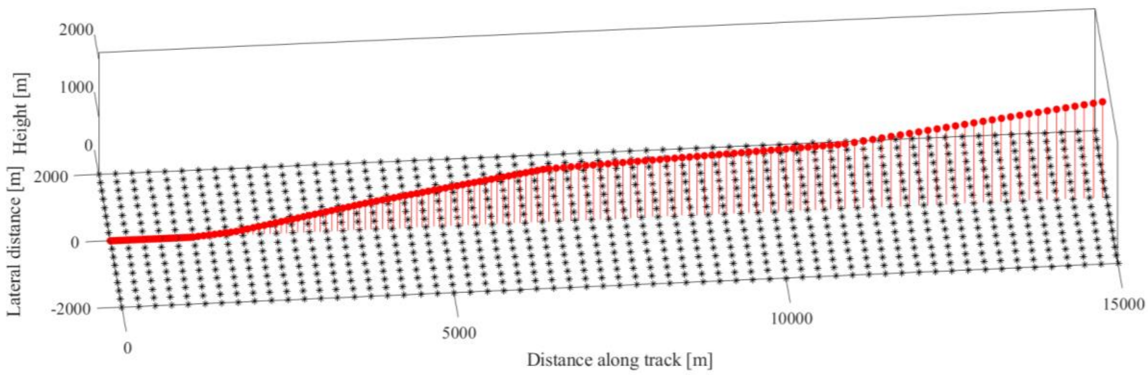

Figure 3.14 Height profile and grid-point for SEL calculations

In each of the grid points, the SELs are calculated using the predictions for the complete flyover. In this way, the basis is formed for a single-event noise contour.

3.2.3. Model output comparison

A way to compare both models is to look at the noise contours corresponding to the calculated grid SEL-values. The calculated SEL-values in each of the grid points for both models are used to set up SEL-contours for a first visual comparison. Both SEL-contours are shown in Figure 3.15.

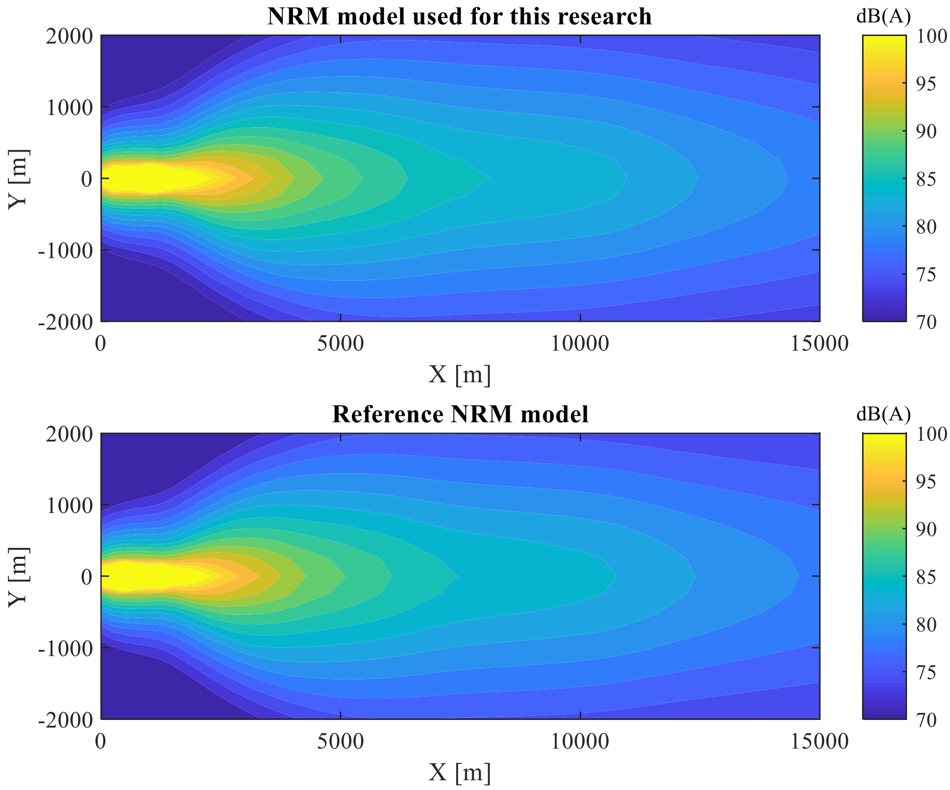

Figure 3.15. Visual model validation: noise contour comparison

In Figure 3.15, it can be seen that these contours have a similar shape and size, implying there are no major deficiencies in the newly implemented model. However, a contour plot does not show individual errors in grid points.

Information on the absolute error for each grid point is given in the scatter plot in Figure 3.16, showing the SEL-values calculated by both models. Preferably, the points should be as close to the equality line as possible, indicating a low absolute error.

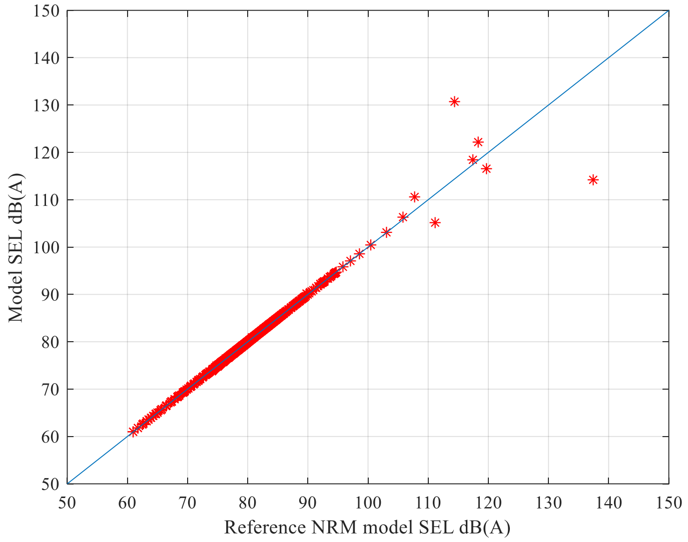

Figure 3.16. Grid point scatter showing the absolute error between both models in each point

Figure 3.16 shows that the SEL-values for most of the grid points lie on the equality-line. For the highest SEL-values, larger deviations are occurring. The points showing the largest deviations correspond to the grid points on the runway. The deviations are the result of the variable timestep that is used in the model by Galis that is not implemented in this model, discussed in section 3.1.5. This has the largest impact on small segments, where the timestep is changed frequently to end up in the segment transition locations, that are close to grid points. For the first segments of take-off, shown in Figure 3.17, this is the case.

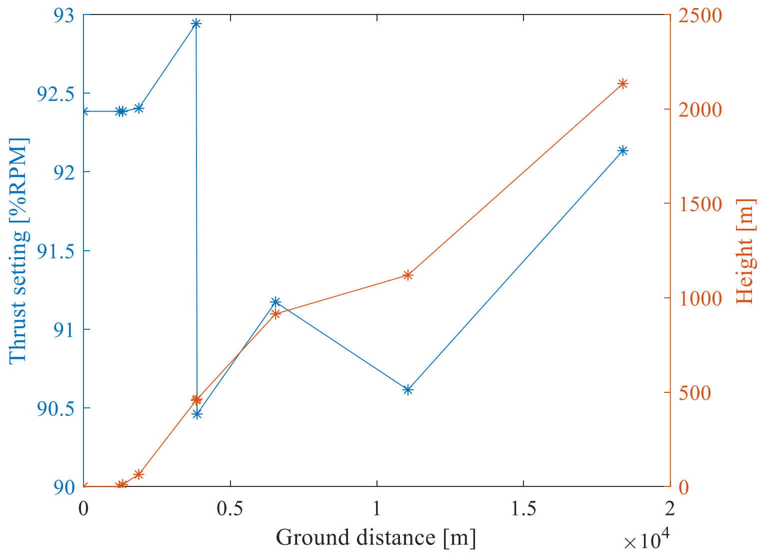

Figure 3.17. Take-off profiles 4690501

Since the locations for which the model will be used are not on or close to the runway, the model can be used reliably in the scope of this research. If this scope changes, the validity of the model for that purpose should be assessed again.

4

NOMOS measurements

This chapter gives an overview of the used measurement data and how this data is acquired. First, information is given about the measurement system and terminal locations. Next, measurement data is visualized and analysed by comparing the NOMOS noise level output with the corresponding sampled audio file for a flyover event.

4.1. Schiphol NOise MOnitoring System (NOMOS)

To compare the modelled noise levels to the measured noise levels on the ground, aircraft noise measurements are used. These measurements are taken by 41 continuously operating Noise Measurement Terminals (NMTs) around Schiphol Airport, called the Noise Monitoring System (NOMOS).

The noise measurement terminals are located in populated areas in the proximity of the Schiphol flight routes. While the local authorities decide on the location of the NMT, the control and management is the responsibility of Amsterdam Airport Schiphol (AAS). All terminals are placed and maintained by Bruël and Kjaer (B&K), a company that is also responsible for the processing and management of the data. An overview of the current NOMOS measurement network is given in Figure 4.1.

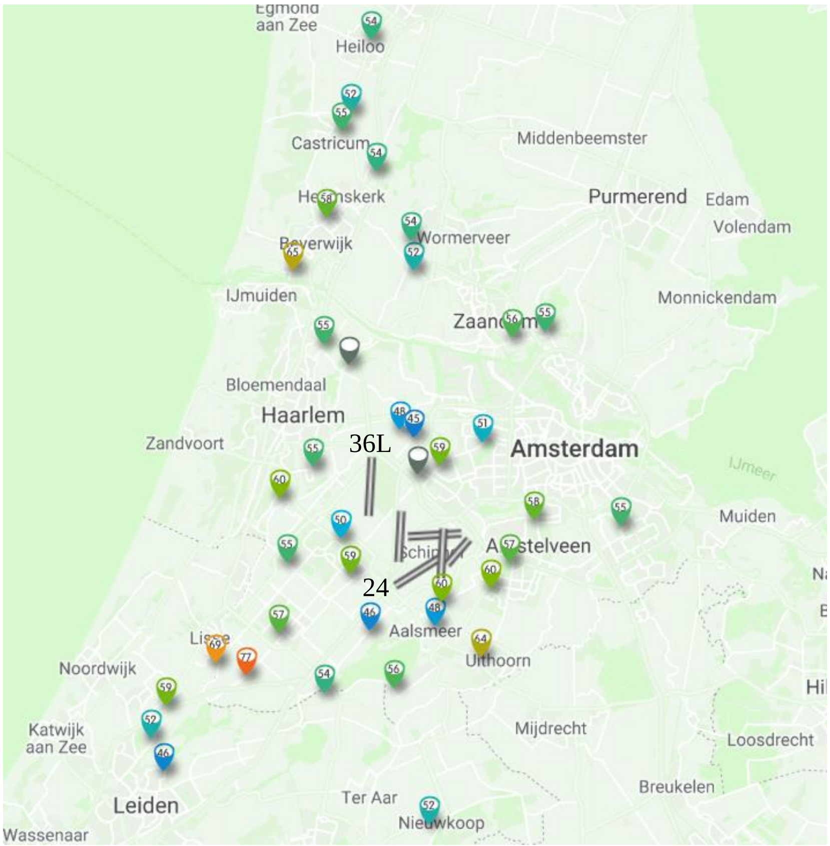

Figure 4.1. Layout of the NOMOS system around Schiphol Airport

Figure 4.1 shows that these NMTs are not only located close to the airport, but also at more remote locations. These more remote locations are under the flight paths of preferential runways 36L/18R (Polderbaan) and 24/06 (Kaagbaan) as becomes clear from the terminals placed in these directions.

Since the specific locations are determined by the authorities, the NMTs are placed in inhabited areas. For this reason, the terminals give a good representation of the noise levels encountered by the community. However, there is usually more background noise in these areas, affecting the measurements. A way to deal with this is to adjust the minimum noise level threshold setting for measurements. This leads to better assigning of noise to aircraft, while on the other hand excluding lower-noise flights.

For this reason, the NMTs in this research are selected based on the criteria that they should be close to the airport and measure clearly distinguishable aircraft noise. In case of doubt, the measurements can be played back from the automatically saved mp3-file.

4.2. NOMOS measurements

The NOMOS NMTs measure the full flyover pressure signal and process this to a 1-second equivalent A-weighted Sound Pressure Level. These time-series are available from the ANOMS database of B&K. An example of two B738 flyover measurements, measured at NOMOS 40 are shown in Figure 4.2.

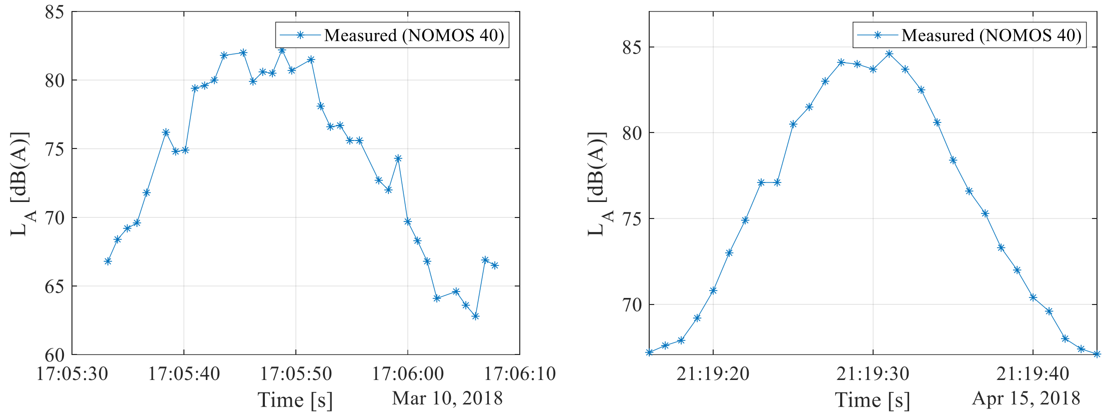

Figure 4.2. B738 flyover measurements by taken by NOMOS NMT 40

Figure 4.2 shows that even though the noise events follow an expected flyover pattern, they can differ significantly in smoothness. One possible explanation for this, which is not tested in this research, is the level of atmospheric turbulence influencing the noise levels up to several dB(A) [12].

Next to the above presented output, the complete time-series pressure signal of the flyover is also sampled and converted to an mp3 audio file.

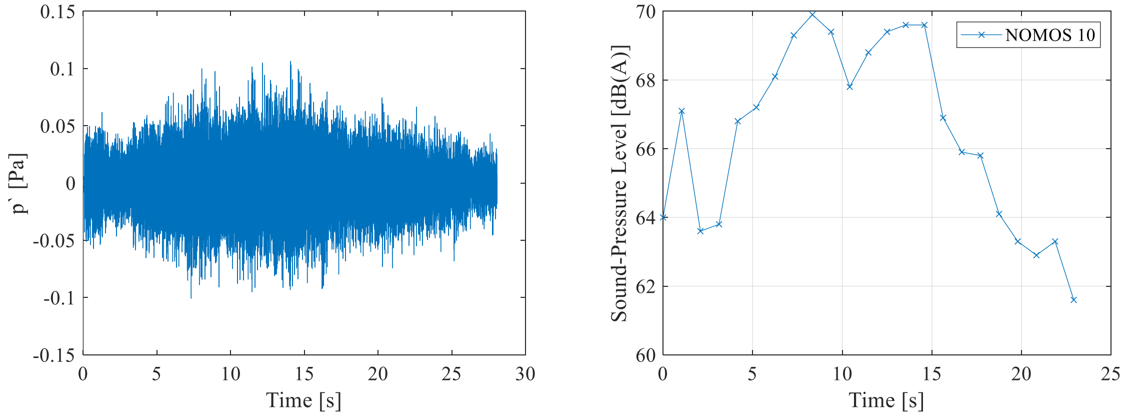

Figure 4.3. Sampled audio file (left) and corresponding measurement (right) from NOMOS

Figure 4.3 shows the audio file and corresponding A-Weighted Sound Pressure Level (L_A) measured at NMT 10 for an Easyjet A320 flyover. Audio files make it possible to playback the noise event, and are in some cases used to verify the measurements. In case of unreliable measurements, for example in duration or shape, the audio can be used to manually distinguish aircraft sound from background noise. In the next part, the audio file is compared to the NOMOS output A-weighted Sound Pressure Levels as given by ANOMS.

To analyse the time-series as shown on the right of Figure 4.3, the pressure signal on the left is divided in a set of equal sized samples and converted to the Power Spectral Densities (PSD), or Power/Frequency, corresponding to the frequency spectrum up to 4000 Hz, as the result of the 8000 Hz sampling frequency (f_s) of the data and the Nyquist Criterion [13]. The PSDs are calculated using a fixed chunk size (N_{fft}) of 400 samples, corresponding to a time-frame of 0.05 seconds, zero-padded to a power of two, 1024, to obtain smaller steps in the frequency domain. Lastly, a Hanning window is applied to decrease the spectral leakage with the trade-off of a slightly lower frequency resolution [14].

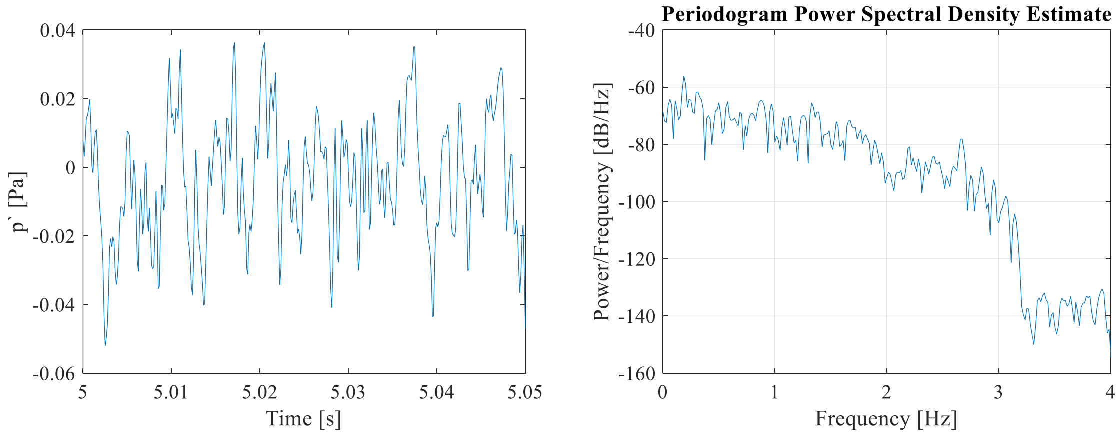

Figure 4.4. 0,05 second sample of the audio file (left) and the Periodogram with estimated PSD (right)

Figure 4.4 shows the PSD corresponding to the timeframe 5,00 – 5,05 seconds. By multiplying the individual PSD values with the corresponding frequency bandwidth (Δf) and summing these results, the effective pressure (p_e) for this time-frame is found. Consequently, the effective pressure for each time-frame is calculated using the Power Spectral Densities from the periodograms using Equation (4.1).

$$p_e^2 = \int_{-\infty}^{\infty} PSD(f)\, df \tag{4.1}$$

The effective pressure is converted to a Sound-Pressure Level (SPL) using the reference pressure ($p_{e,0}$) squared and taking the 10-based logarithm as is shown in Equation (4.2).

$$SPL = 10\log_{10}(\frac{p_e^2}{p_{e,0}^2}) \tag{4.2}$$

Applying this to the measured mp3 signal of the flyover, the instantaneous Sound-Pressure Levels for each 1 second timespan are calculated and compared to the A-weighted NOMOS output shown in Figure 4.5.

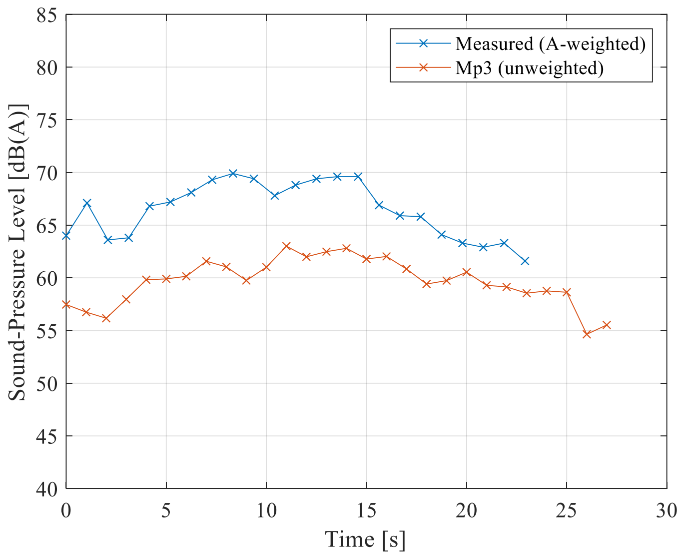

Figure 4.5. Measured (A-weighted) SPL compared to the (unweighted) SPL from the audio file

Both NOMOS and NRM calculate noise levels using A-weighting. This A-weighting corrects for the sensitivity of the human ear to different frequency components in the sound according to the equal loudness contour of 40 phon, where phon is a measure of loudness. The loudness contours accounts for the sensitivity of the human ear, which decreases significantly with decreasing frequency. For example, a 40 dB SPL tone at 1000 Hz is perceived equal loud as an 80 dB SPL tone at 30 Hz.

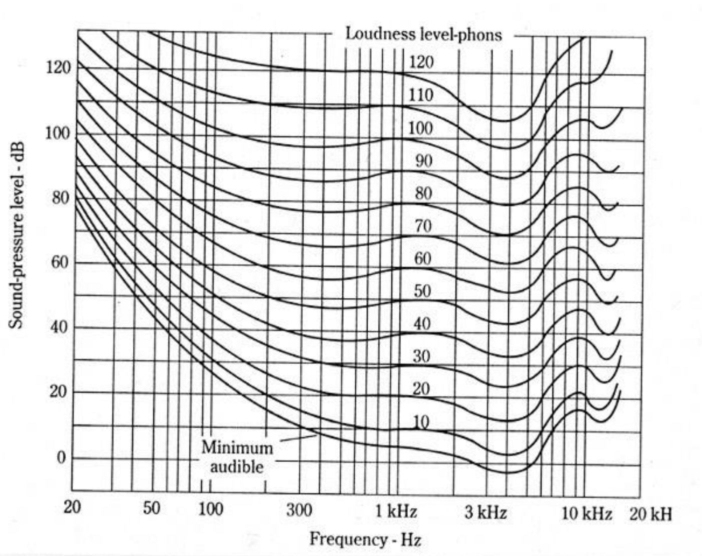

Figure 4.6. Equal loudness contours (Rochester University)

Figure 4.6 shows the phon lines indicating equal loudness for a combination of frequency and Sound-Pressure Level. This figure confirms that low frequencies, up to 400 Hz, allow for a higher Sound-Pressure Level for equal perceived loudness.

The A-weighting correction that follows from this 40 phon line is given in a third-degree polynomial as a function of frequency (f) in Equation (4.3).

$$\Delta L_A(f_c) = -145 + 98.262 \log_{10}(f_c) - 19.509 \log_{10}(f_c)^2 + 0.975 \log_{10}(f_c)^3 \qquad (4.3)$$

To visualize this relation with frequency, it is plotted between the thresholds of human hearing from 20 Hz to 20 kHz in Figure 4.7.

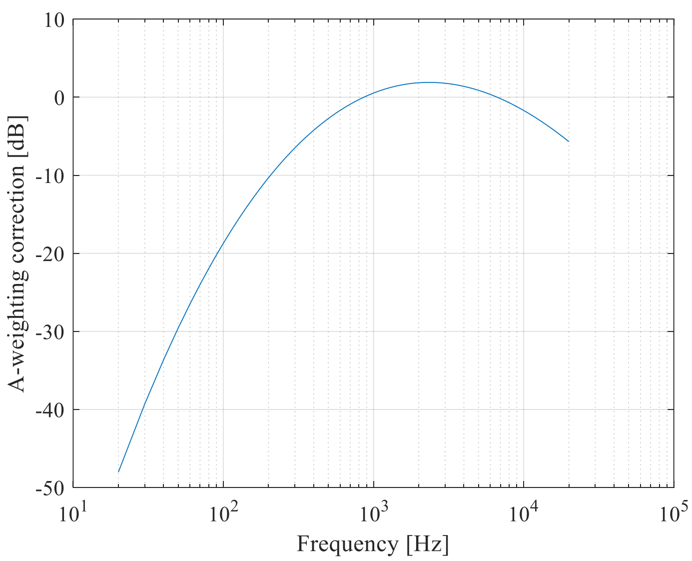

Figure 4.7. A-weighting correction for the audible frequency spectrum

Figure 4.7 confirms the large effect of the frequency on the Sound Pressure Level correction using A-weighting. From 20 to 860 Hz, a negative correction if applied to the measured Sound Pressure Level. Between 860 and 6660 Hz, the correction is positive up to 1,9 dB before dropping below zero again for higher frequencies.

The A-weighting correction is applied to the Power Spectral Densities as shown in Figure 4.4. The A-weighting correction for each center frequency f_c corresponding to the frequency bands is added to the SPL.

$$L_A = 10\log_{10}\left(\sum_{f_c} 10^{\frac{SPL(f_{c,i})+\Delta L_A(f_{c,i})}{10}}\right) \tag{4.4}$$

As a result, the 1-second A-weighted Sound-Pressure Levels are used to assess the mp3-signals, sampled at 8000 Hz, to the NOMOS output. Both A-Weighted Sound Pressure Levels are shown in Figure 4.8.

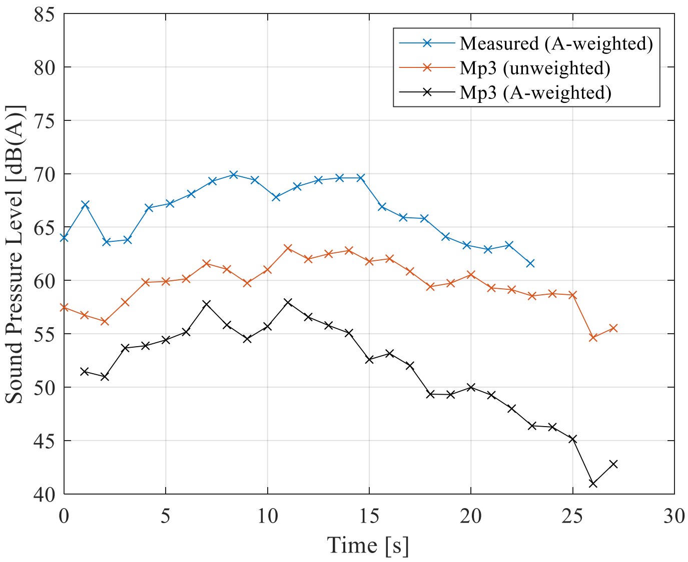

Figure 4.8. Audio file A-weighted Sound Pressure Level compared to the measurement

Figure 4.8 shows that both the NOMOS output and the calculated L_A from the audio file show a similar trend. However, the results from the audio file are more than 10 dB lower for the entire timespan. This is the effect of the information that is lost when compressing the full-size digital audio measured by the NOMOS NMT to the mp3 audio file. Where the NMT uses a 48 kHz sampling frequency, the compressed mp3 audio file is down sampled to 8 kHz to reduce the size of the file. This results in a 'loss' of information above 4 kHz, conform the Nyquist Criterion, up to the 24 kHz of the full-size data that is used to calculate the NOMOS L_A.

From this, it becomes clear that a lot of important information got lost from the compression and the mp3 audio files are not useful for direct validation of the NOMOS output noise levels. In case this is requested, the full samples should be taken directly from the NOMOS NMT at the moment of the flyover. However, the mp3 audio files contain information about the sound frequency spectrum, which will be used later in Chapter 6.4.

5
Research Setup

5.1. Analysed flights

Based on the weather conditions as mentioned in Section 3.1.4, a set of flights is filtered out from the total number of flights in 2018. The data and profiles used in NRM are set up for International Standard Atmosphere conditions, which are assumed to correspond well to the average weather conditions in the Netherlands. However, on an individual basis, the weather conditions can deviate significantly from these standards. To minimize the weather effects on the analysis, thresholds have been set around the standard ISA-conditions to end up with a meteo-window for which the flights are analysed. The thresholds are tabulated in Table 5.1 [4].

Table 5.1. Meteo-window with thresholds to filter the flights

	ISA-conditions	Threshold
Ambient pressure, p_a	$1013\ hPa$	$980\ hPa < p_a < 1050\ hPa$
Ambient Temperature, T_a	$15\ °C$	$13\ °C < T_a < 16\ °C$
Relative humidity, Φ	$70\ \%$	$60\ \% < \Phi < 80\ \%$
Wind speed, V_w	$0\ m/s$	$V_w < 2\ m/s$
Rain	$none$	$0\ mm$

The time-frames corresponding to the thresholds in Table 5.1 are derived from the weather data in ANOMS, measured by the NOMOS network on multiple locations around the airport. These weather stations sample continuously and give the average weather conditions over a 30-minute timespan. Based on these average conditions, the timespans are selected.

Within these timespans, 4862 flights are found, spread over all runways for the year 2018. The 4/3-class is representing 2396 of the 4892 flights, approximately 50%. As a result of the large variety in airlines and procedures, flights are only analysed for KLM, Transavia (TRA), Lufthansa (DLH) and Easyjet (EZY). For these airlines, the starting procedure and aircraft configurations are known. Because these airlines are most predominantly present at Schiphol airport, this results in a total of 1538 flights out of the 2396 flights, approximately 64%. For the analysed runways 18L and 36C, this results in 440 and 275 starts respectively. An overview of the total filter procedure is shown in Figure 5.1.

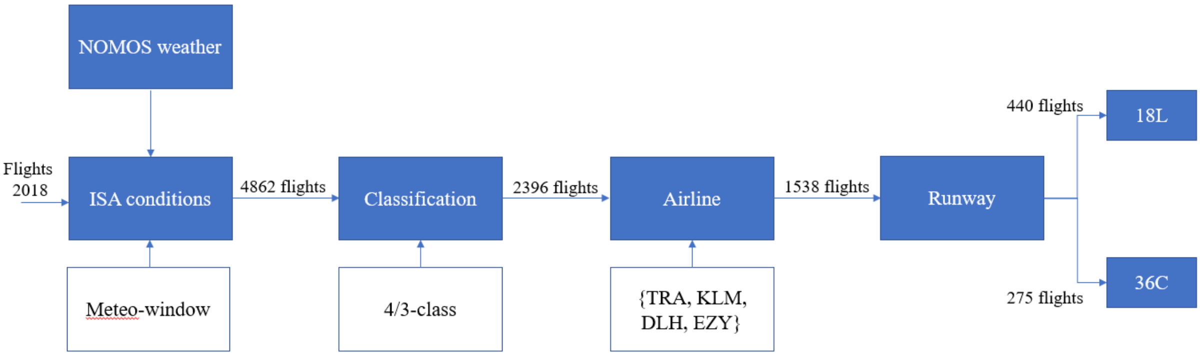

Figure 5.1. Flights filter procedure overview

A more detailed overview of the airlines and number of flights per type for both runways are given in Figure 5.2.

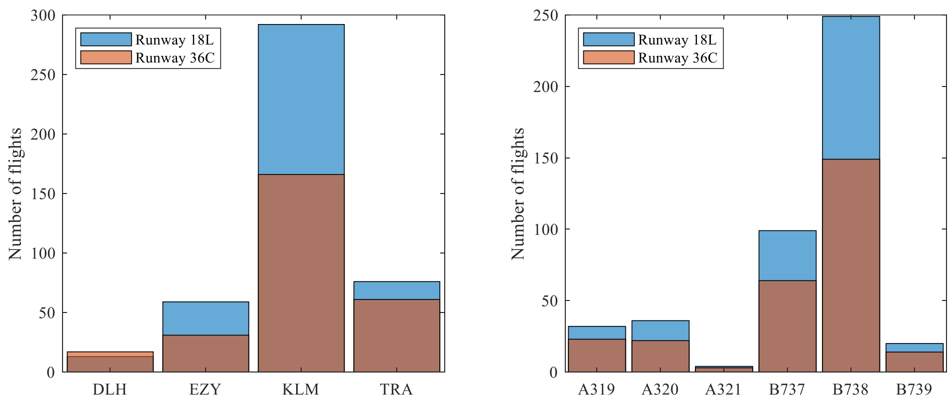

Figure 5.2. Distribution of flights over airline (left) and aircraft type (right)

From Figure 5.2, it is found that KLM represents the largest number of flights for both runways. Furthermore, the B738 accounts for around 50% of all the flights in this class. Because of this, the total sound exposure of the class will be dominated by the B738.

For the analysis, only the A319, A320, B737, B738 and B739 are used as all these aircraft occur at both runways for the selected flights. The A321 does not occur at runway 18L for this selection and is for runway 36C only present with several flights and is for this reason left out of the analysis.

5.2. Track modelling

To get an overview of the flown flight tracks, the ground tracks corresponding to the filtered flights are shown for both runways in Figure 5.3. These flight tracks, including ground track and height, are provided by LVNL and are extracted from the ARTAS radar data as is discussed in section 2.3.

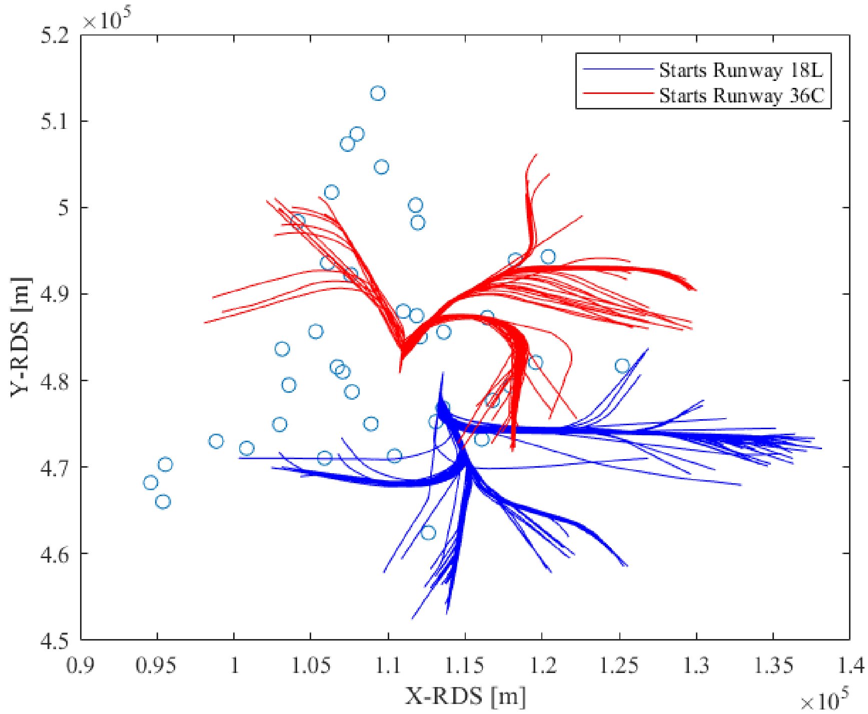

Figure 5.3. Ground tracks of the used flights

As can be seen in Figure 5.3, the majority of the flights follow specific flight routes. However, there are deviations from these flight routes dependent on the destination of the flight. These deviations make calculations with the average theoretical ground track, as is usually the case for NRM, less reliable in single event comparison of the flight with measurements. For this reason, it is chosen to calculate with the individual ground tracks for all of the selected flights.

These ground tracks can be linked to the prescribed height profiles in two ways: using the speed corresponding flight profile table (Figure 3.2) to link the profile height to a time, or using the profile distance to link the profile height to the track distance. Linking the profile height to the track distance, an equal rate-of-climb as a function of distance is considered for the track and the profile. The example of this is shown in Figure 5.4.

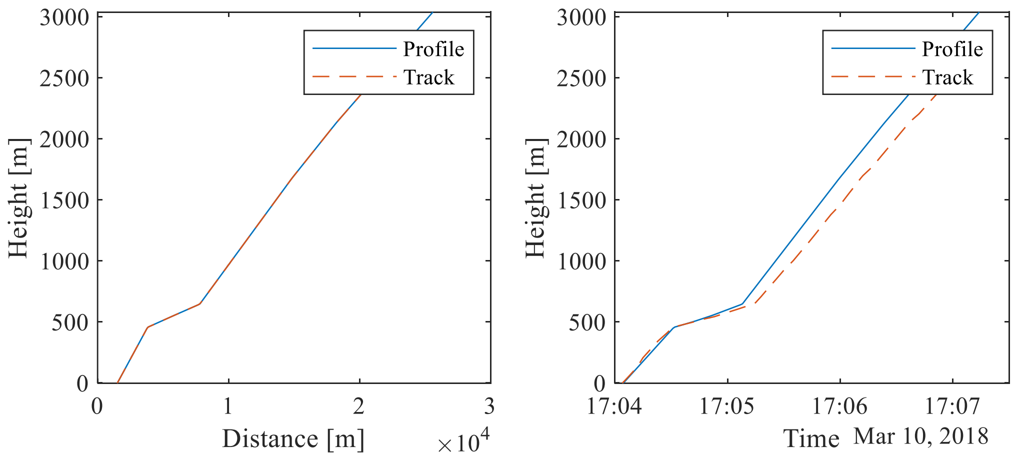

Figure 5.4. Height profiles matched to ground profile for distance (left) resulting in a time-lag (right)

Figure 5.4. shows that there is a slight mismatch between the real track height and the theoretical profile height over time. This is the result of a different real ground speed compared to the theoretical ground speed that is prescribed in the profiles. This deviation in ground speed

is shown by looking at the ground distance travelled over time, for both the track and theoretical profile, in Figure 5.5.

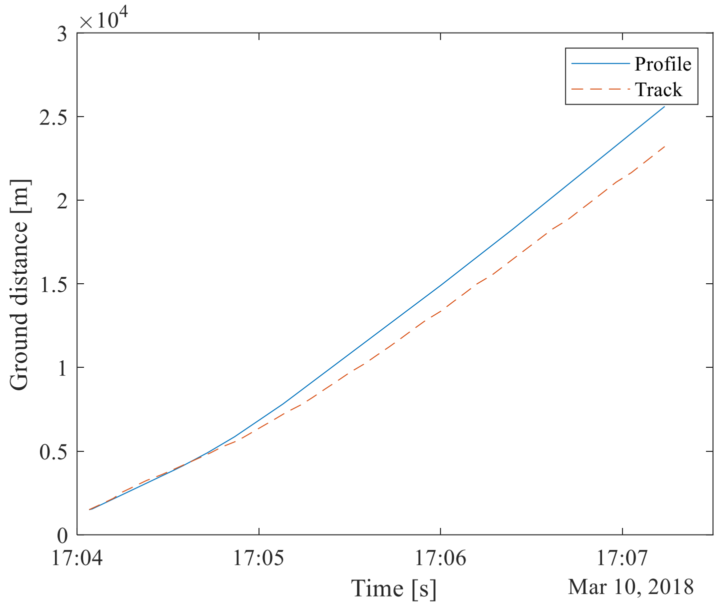

Figure 5.5. Ground distance travelled over time for track compared to profile

Figure 5.5 shows that the track lags behind on the profile in terms of distance travelled, originating from a lower real (track) ground speed. This lower track ground speed results in a longer noise event duration.

5.3. Analysed NOMOS Noise Measurement Terminals

As a result of the selected runways, a selection of NMTs is used for comparison of calculations with measurements. The NMTs are selected for both runways based on their location with respect to the flight path and their distance from the take-off, to reduce undetected flights or influences of background noise.

The measured noise events are linked to aircraft flyovers based on the maximum noise level and the closest distance of the aircraft to the NMT. First, the aircraft track times, in emission time, are converted, to reception times of the sound at the location of the NMT using the distance to the NMT. Based on the closest distance of the aircraft to the NMT, a first guess is made of the reception time at which the maximum noise level is expected at the NMT. This maximum noise level time guess is then linked to the time of maximum noise measurement by the NMT. If both timestamps have a maximum of 15 seconds offset, the events are assumed to be correlated. Else, if no noise event is found within this 15 second timespan, no noise event is correlated to the flight for that NMT.

For Runway 18L, NMTs 40, 10 and 25 are used. These NMTs are located close to the ground paths of all analysed flights starting from 18L as shown in Figure 5.6.

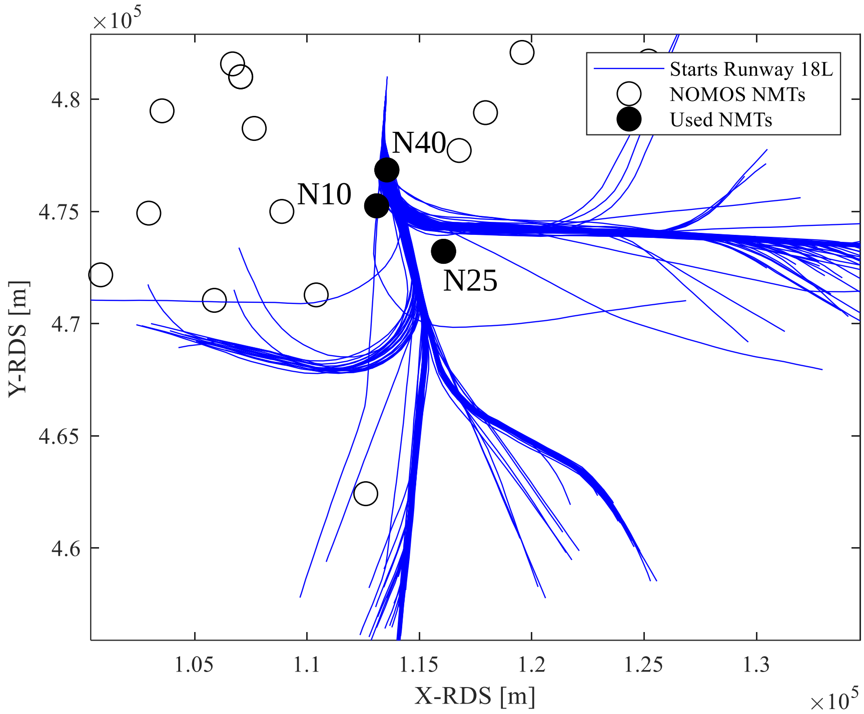

Figure 5.6. Runway 18L: Location of NOMOS NMTs with respect to analysed flights

The NMT that is the closest to the runway is number 40, located just outside of Aalsmeer at the Oosteinderweg. At this location, the largest number of correlated events should be found as all flight tracks fly over this location independent of destination. The same holds for number 10, located in the Clussiusstraat in Aalsmeer. From this location, the air traffic starts to bound towards their routing point dependent on the destination. This becomes clear when looking at number 25, located in Uithoorn between two main routes towards the east (REN1E, ARN3E, AND2E) and south (KDD1E, BER3E, LOP3E, VAL3E) from where traffic can bound north or west respectively. An overview of the number of aircraft per type is measured at each NMT as a result of this traffic is given in Table 5.2.

Table 5.2. Runway 18L: Number of correlated noise events per NMT for each aircraft type

	B737	B738	B739	A319	A320
Total started	99	249	20	32	36
NMT 40	98	248	20	32	35
NMT 10	99	247	20	31	36
NMT 25	73	212	19	20	22

From Table 5.2, it can be seen that close to the runway, the largest number of events can be correlated to a flight. However, when moving further away from the runway, the number of correlated events decreases, as is found for NMT 25. As the noise levels decrease further from the airport, these flights do not surpass the noise level thresholds set at the NMT.

The second runway that is used is 36C, a take-off in northern direction. For this runway, measurement terminals 92, 35 and 2 are selected.

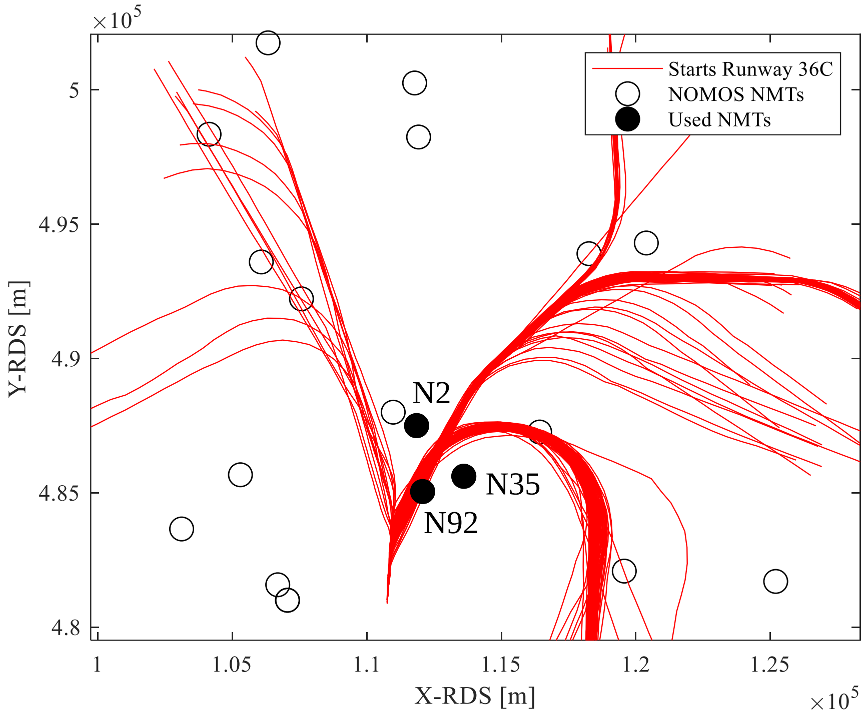

Figure 5.7. Runway 36C: Location of NOMOS NMTs with respect to analysed flights

From Figure 5.7, it is seen that the 3 NMTs that are chosen lie close to the main departure route in north-eastern direction. Before crossing NMT 92 at Lijnden, a small section of the flights is diverted in north-western direction (BER3V, GRL3V). The major part of flights takes off in north-eastern direction (NSU1W, IVL2W, NYK3W, OGI2W, WDY1W) and crosses the selected NMTs. After NMT 92, traffic with a southern destination starts making a turn towards this direction around NMT 35. NMT 2 lies between both main routes and should, because of this, be able to capture most of the noise events corresponding to the selected flights. As NMT 92 and 35 are located at the east of the north-eastern route, it is harder to capture the noise events corresponding to the north-western flights.

Table 5.3. Runway 36C: Number of correlated noise events per NMT for each aircraft type

	B737	B738	B739	A319	A320
Total started	64	149	14	23	22
NMT 92	63	149	14	23	22
NMT 35	54	127	12	14	16
NMT 2	62	149	14	20	19

Table 5.3 shows that for NMT 92 and 2, most of the flights can be linked to a noise event measured by the NMTs. Since NMT 92 is close enough to take-off, it does not have complications with capturing the north-western traffic. However, for NMT 35, the location further from take-off and more to the east does result in a lower number of events being captured by the NMT.

6
Results and discussion

This chapter presents and analyses the results of the research. First, individual flights are modelled and compared to NOMOS measurements, using both noise level time-series, to illustrate errors that occur at a detailed scale. Next, the aforementioned larger set of flights is modelled and compared to NOMOS measurements based on the SEL to assess type-specific errors between calculations and measurements occurring at a larger scale. Still, at this stage, no conclusion can be drawn regarding the accuracy of the model calculations, as there are also errors occurring between modelled profiles and reality at the input side of the model. Therefore, the differences between model input and reality are analysed and reduced by replacing theoretical height and thrust profiles by real tracks and derived engine settings. Lastly, possible other sources for errors will be discussed, focussing on the aircraft type specifications.

6.1. Single event comparison with NOMOS

In this first step, the model is compared in detail to the measurements taken by the NMTs. In this way, similarities and differences between theoretical (modelled) noise levels and real noise levels over time are visualized. The model is capable of calculating complete noise events, i.e. noise levels over time $L_A(t)$ which can be compared to the time-series measured by the NMT.

For this analysis a B738 flight is used, departing from 18L in southern direction, passing by NMT 40, 10 and 25. The corresponding flight profile is visualized in Figure 6.1.

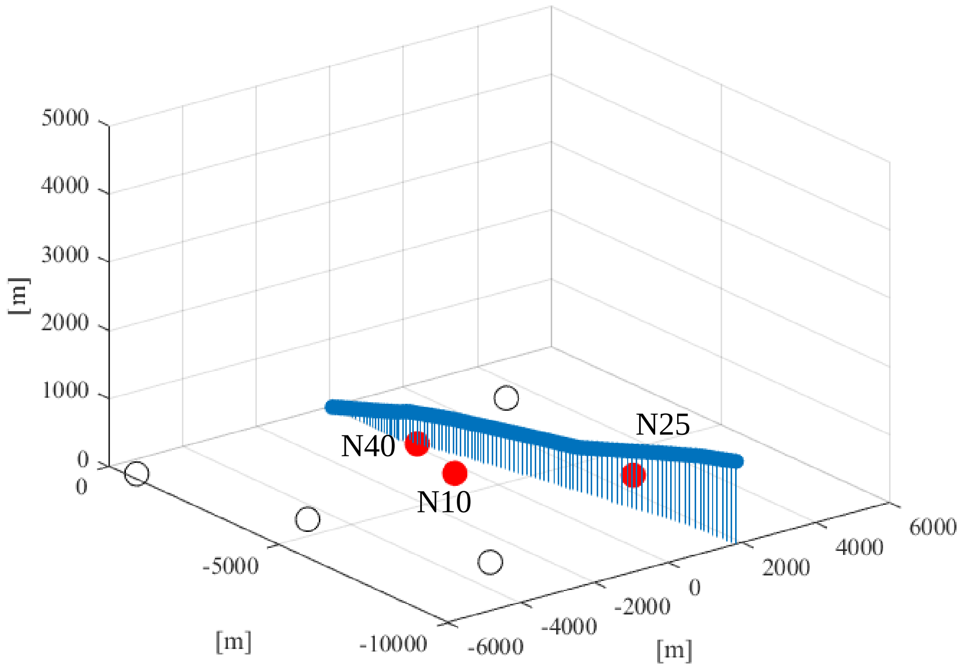

Figure 6.1. 3D reconstructed flight 18L

The ground profile in Figure 6.1 corresponds to the real ground track that is flown, following from the radar-data, where the height profile is a standard theoretical height profile.

The thrust setting is linked to this height profile and is used together with this ground- and height-profile to calculate the noise levels at the specific locations of the NMTs.

The noise levels are calculated for the location of NMT 40 and 10 and compared to the measured noise levels in Figure 6.2

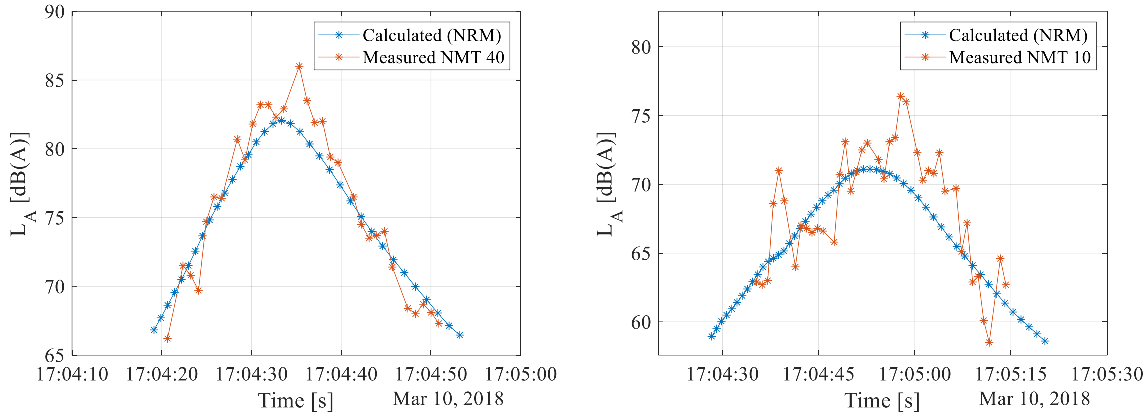

Figure 6.2. Single event: calculations compared to measurements for NMT 40 (left) and NMT 10 (right)

From the left graph in Figure 6.2 it is found that the modelled and measured noise levels for NMT 40 follow the same pattern. This NMT is located close to the take-off location and directly under the flight path, resulting in a small lateral attenuation effect. The measured curve is close to the ideal situation with only relatively small fluctuations. The measured peak noise level is higher than the calculated maximum noise level, being 86 dB(A) and 82 dB(A) respectively. This is strongly contributing to the higher measured SEL (94.1 dB(A)) compared to the calculated SEL (92.2 dB(A)).

For NMT 10, some clear differences can be found compared to NMT 40. In this situation, the fluctuations are much larger than for NMT 40 causing the noise event not to follow the expected pattern properly. Furthermore, the maximum measured noise level of 76.4 dB(A) is again higher than the modelled maximum noise level (71.1 dB(A)) and occurs a couple of seconds later than expected from the model. This results again in a higher measured SEL (86.2 dB(A)) than calculated SEL (84.2 dB(A)).

Comparable results are found for another B738 flight, flying the same flight route. The calculated and measured noise levels at NMT 40 and 10 for this flight are shown in Figure 6.3.

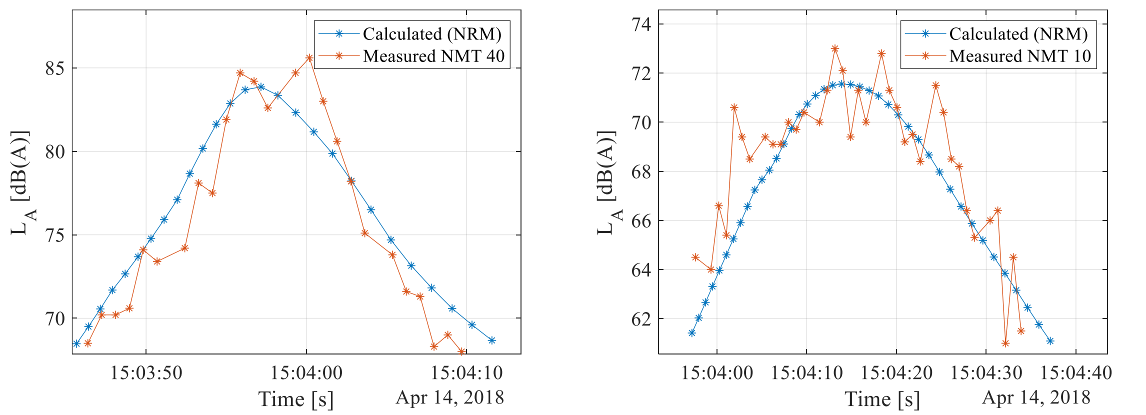

Figure 6.3. Single event (2): calculations compared to measurements for NMT 40 (left) and NMT 10 (right)

Again, both maximum calculated noise levels underestimate the measured maximum noise levels up to several dB(A). Even though the measured noise levels for NMT 40 are lower than the calculated noise levels for the largest part of the event, the measured SEL is still 0.9 dB(A) higher than the calculated SEL. This shows how the large influence of the maximum noise levels on the SEL. NMT 10 shows the same large fluctuations as were visible in Figure 6.2. However, when comparing modelled and measured SEL for NMT 10, only a difference of 0.5 dB(A) underestimation in SEL is found compared to the measurement.

From this detailed single event comparison, it becomes clear that the model and measurements follow the same trend. This trend is better visible for NMT 40 than for NMT 10 as a result of the fluctuations that strongly influence the measurements at NMT 10. Next to this, the maximum measured noise level is for all 4 events higher than the calculated maximum noise level. This strongly effects the resulting SEL causing the measured SEL to be higher than the calculated SEL.

6.2. Multi event comparison with NOMOS for theoretical input

To evaluate the effect of these differences between calculations and measurements for all individual aircraft types within the class, the same comparison is done for the entire set of flights based on the SELs. Each modelled noise event is coupled to a measured noise event at the selected NMTs for the specific runway.

The results are visualized in scatter plots, each showing the calculated and measured SEL for all flights captured by the NMT. The results are subdivided into the 5 selected aircraft types. In case of a good classification, measurements should be equal to calculations for all types and no specific clusters of types can be distinguished. In the ideal situation, all flights are located close to the line with slope one (measurement equal to calculation). The results for the 440 starts on runway 18L are shown in Figure 6.4.

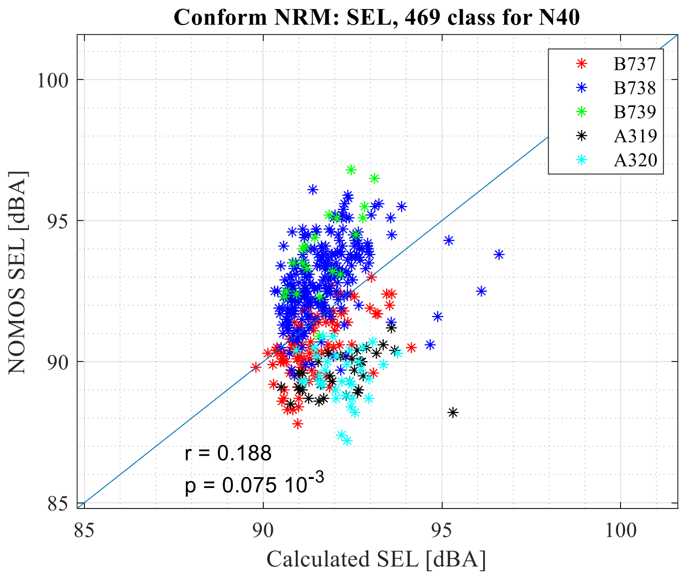

Figure 6.4. Profile results: SEL calculations vs measurements for NMT 40

From Figure 6.4, clustering of specific types becomes visible. Where clusters for the B738 and B739 are clearly above the line, measurements higher than calculations, the B737, A319 and A320 are under the line, i.e. the measurements are lower than the calculations. As each data-point has a calculated (SEL_{calc}) and measured (SEL_{meas}), the difference in average SEL ($SEL_{diff,avg}$) can be calculated for all flights (N) (Equation (6.1)).

$$SEL_{diff,avg} = \frac{\sum_N SEL_{calc,i} - SEL_{meas,i}}{N} \tag{6.1}$$

The differences between the calculated SEL and measured SEL as found from Figure 6.4 are shown in Figure 6.5.

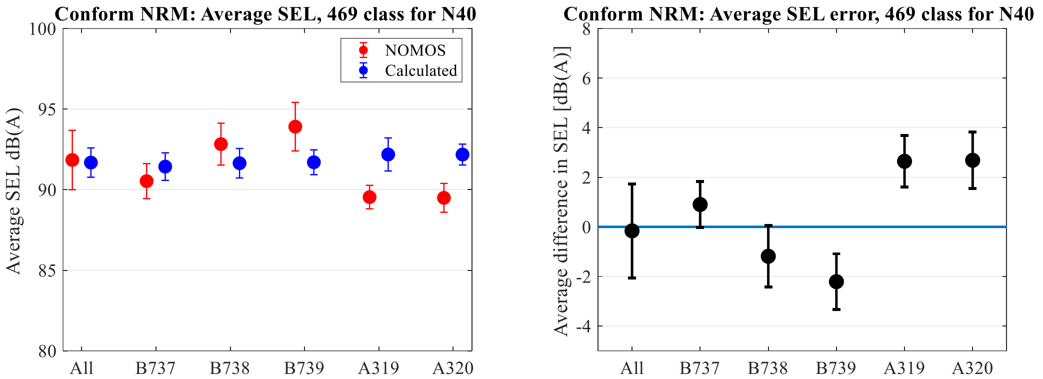

Figure 6.5. Profile results: Average SEL (left) and average error (right) with respect to measurement

In Figure 6.5, the horizontal line through the origin indicates the line for which $SEL_{diff,avg}$ is zero. For results located above this line, the model is on average overestimating the SELs compared to the measurements and vice versa. For the total results, an under 0.5 dB(A) underestimation is found. However, by looking at type-specific errors, this clearly shows that both of the Airbus aircraft are located above the line and measured noise levels are overestimated using the model. The Boeing aircraft show a distribution of the results. Where for the B737 the measurements are overestimated, the model underestimates the measurements for the B738 and B739.

The same procedure is repeated for all 6 NMTs corresponding to runway 18L and 36C in Figure 6.6.

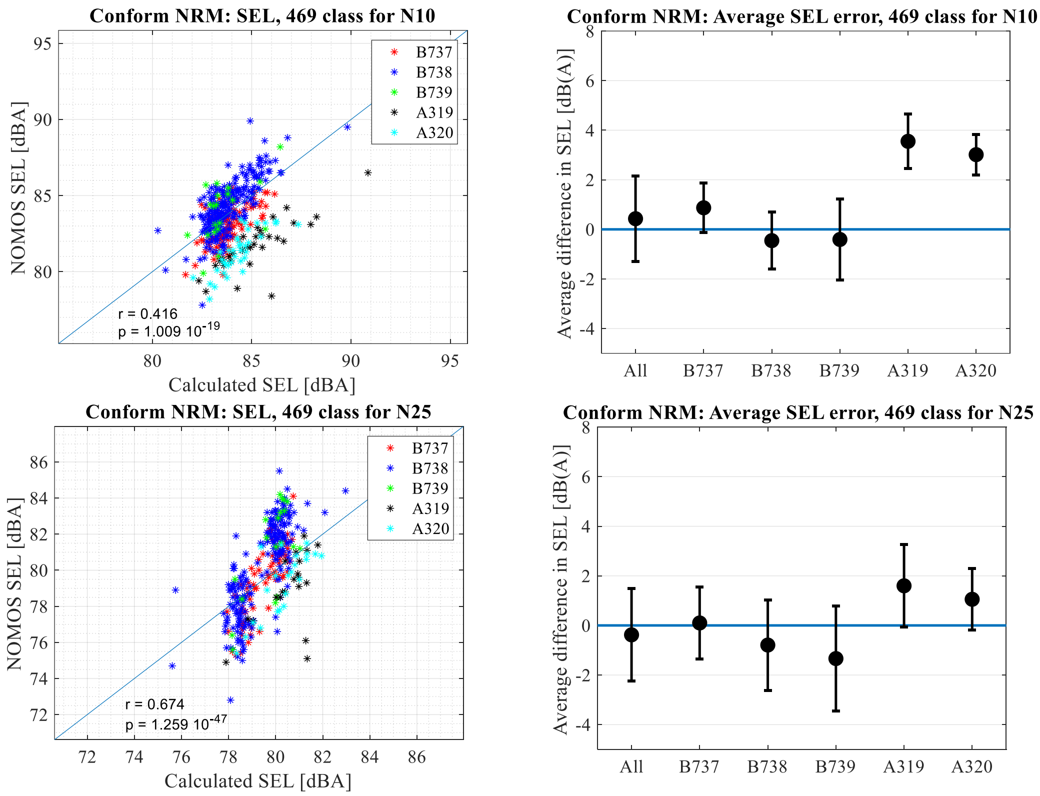

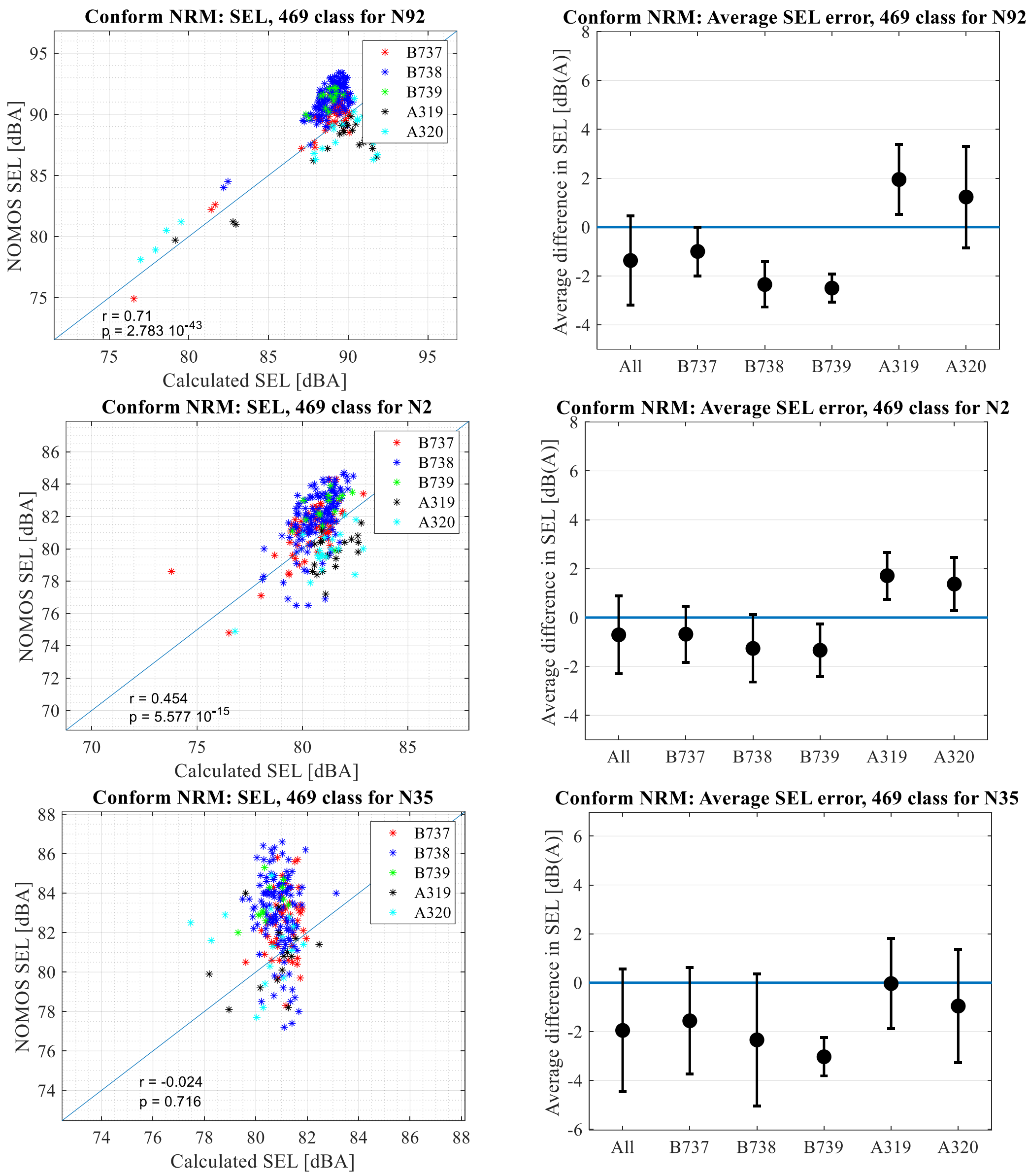

Figure 6.6. Conform NRM: SEL calculations vs measurements for all 6 NMTs (left) and difference of average calculated SEL with respect to average measured SEL (right)

The same pattern is found for most of the NMTs. Where for both Airbusses the SELs are on average overestimated using the model, the B738 and B739 are underestimated. The B737 is located close to the line, with no consistent under- or overestimation of the SELs for all NMTs. Contrary to this pattern, NMT 35 is showing an underestimation of the SELs for all aircraft types. This is the result of the NMT being located close to a busy road, capturing noise events related to road traffic together with the aircraft related noise. This also explains the large spread in measured SELs, from 77 up to 90 dB(A) and the correlation coefficient being close to zero. For most of the NMTs, low correlation coefficients are found showing that the measurements and calculations are weakly correlated. In the ideal situation, the correlation coefficient should be as close to 1 as possible to have all data-points as close the equality line as possible.

From these results, it can be concluded that by only looking at the complete class, the error is only small (up to 1 dB(A)) for the current fleet mix. However, when looking at type specific errors, there is a clear division between types consistently being under- and overestimated by the model. This shows that purely looking at the classification as is prescribed by the guidelines, the types within the class do not show the same behaviour. Concluding, it is found that the classification as is does not provide the requested results as the type-specific errors show to large, and consistent, differences.

To better evaluate these type specific errors, the used input height profiles should be compared to the real height profiles following from the track-data. Furthermore, the model engine settings should be compared to the real engine settings as both height and engine setting are interconnected by equations of motion. Both effects will be analysed and corrected for in the following chapters.

6.3. Effect of flight height

This section evaluates the effect of the deviation of the track height from the prescribed profile heights as are used in the previous calculations. First, the magnitude of the deviation is assessed, estimating the possible error on the noise levels as a result of this. After, the calculations will be done by implementing the track height in the model, replacing the profile height.

6.3.1. Track deviation

The reconstructed flight in Figure 6.1 showed that the calculations are based on a real ground track, combined with a theoretical height-profile. Issues in the matching process occurred as a result of the difference in real and theoretical ground speed. To correct for this, the profile height is matched to the ground track based on the distance the distance travelled as discussed in Chapter 5.2.

The use of the theoretical profiles assumes an average height profile and thrust setting, which can differ significantly on a single event basis. Differences in the height profile lead to a wrong calculation of the straight distance from the aircraft to the observer, resulting in a wrong input to the NPD-tables and an under- or overestimation of the noise levels. Furthermore, this influences the lateral attenuation as the angle between the aircraft and the ground with respect to the observer's location changes.

The individual real track heights are compared to the used profile height for the aircraft using procedure 06, distributed over the occurring distance classes, in Figure 6.7.

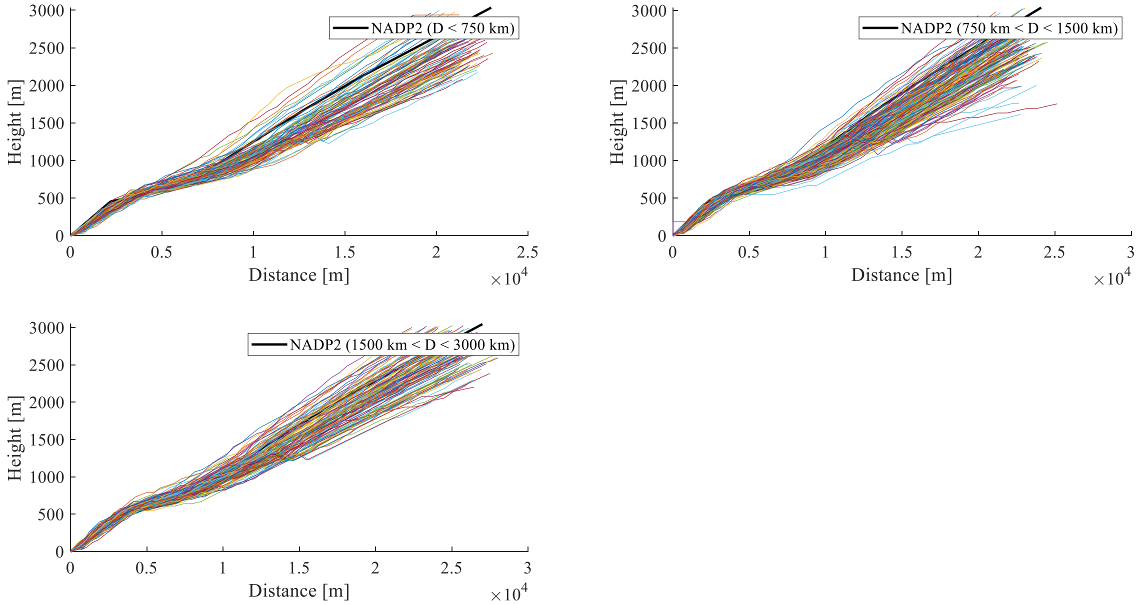

Figure 6.7. Real individual track heights compared to theoretical profile for 3 distance classes

From Figure 6.7, it can be seen that the flights follow a comparable profile, with a distribution around the theoretical profile, shown as the black thick line, as a result of deviations in individual flights. There are multiple possible explanations for deviations such as curved flight paths, reducing rate of climb, or different thrust settings, as will be discussed in Chapter 6.4. To get a better overview of how these individual deviations work out on the total of flights, the average track heights per aircraft type are shown for procedure 06 and distance class 01 in Figure 6.8.

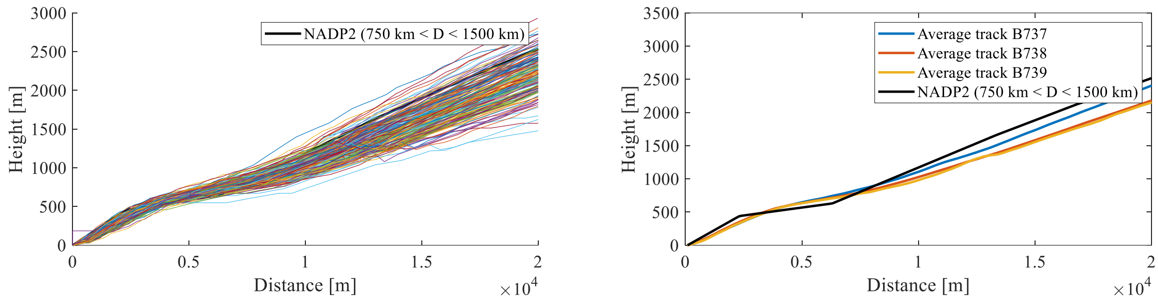

Figure 6.8. Comparison of complete set of individual tracks (left) and type-specific average track height (right) to the theoretical profile for distance class '01'

Since the Airbus aircraft are stated to use procedure ‘07’ (NADP2 1000ft), these aircraft are not included in Figure 6.7 and Figure 6.8. However, when looking at the real average track heights, the procedure overlaps with the Boeing aircraft flying procedure ‘06’ (NADP2 1500ft) as is shown in Figure 6.9.

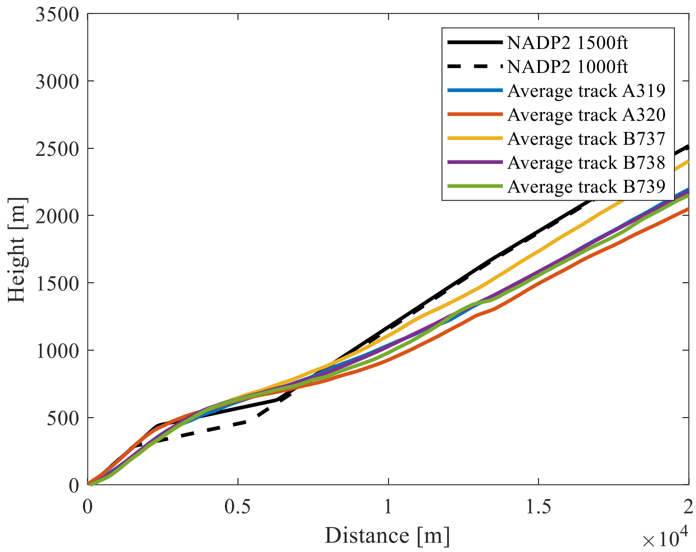

Figure 6.9. Comparison of type-specific average track heights to the NADP2 profiles

From Figure 6.9, it is found that the average track heights indeed match better with the ‘06’ procedure. Corrections for the flight height will for these aircraft types thus result in larger corrections than for the Boeing aircraft.

Furthermore, Figure 6.9 shows that the average track heights for these aircraft types differ from the profile height which is used in the calculations. The magnitude of this deviation is used to illustrate the possible effects on the maximum noise levels under the flight track, on the ground path. The maximum noise levels at the locations on the ground track can be evaluated as the straight distance from aircraft to observer is for these points only dependent on the height. For lateral locations, the lateral distance influences the attenuation and straight distance from aircraft to observer as well. For this reason, only the maximum noise levels, occurring directly under the flight path, are considered in the next steps.

The difference between average track and profile height, following from Figure 6.9, is visualized in Figure 6.10.

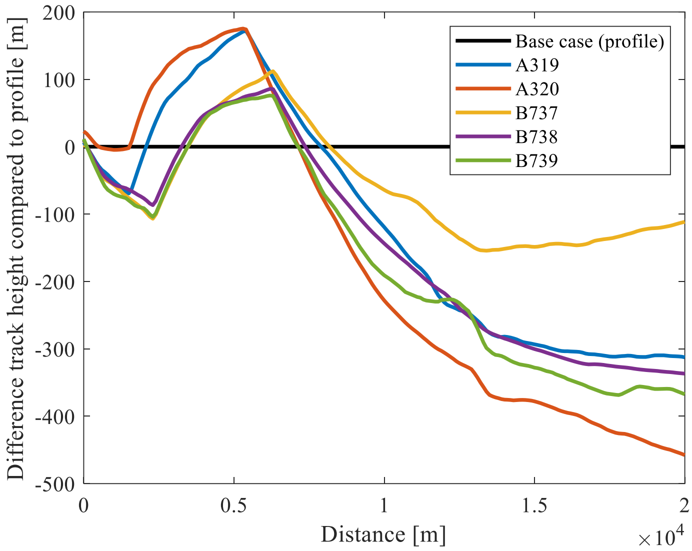

Figure 6.10. Absolute deviation of type-specific average track height from theoretical profile

Figure 6.10 shows negative values where the track height is lower than the profile height and vice versa. The difference in height follows the same pattern for all aircraft in the early stages of the take-off. For the majority of the flight path, the profile overestimates the height of average track, leading to underestimation of the noise levels. It also shows the part of the track for which the profile height underestimates the average track height at a distance between 3500 m and 7500 from take-off, for which the noise levels will be overestimated. However, because the profile is increasing in height, the relative error decreases further from the runway. The relative height of the tracks with respect to the profile are shown in Figure 6.11.

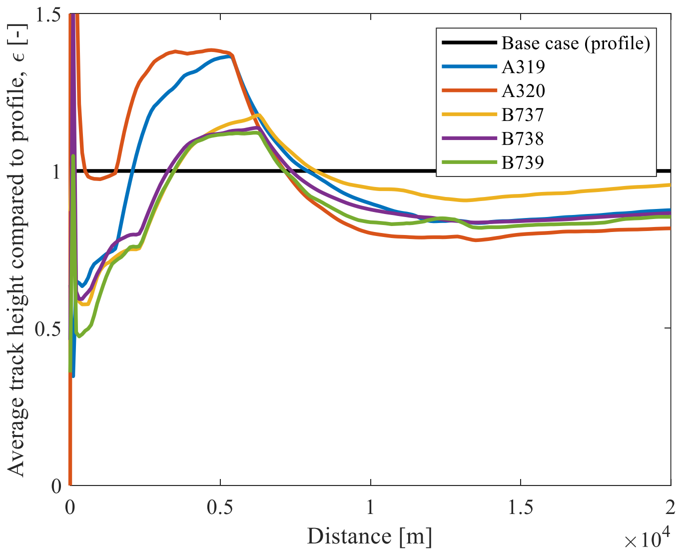

Figure 6.11. Relative height of type specific average track compared to theoretical profile

The relative height factor (ε) in Figure 6.11 can be used to correct the Sound Pressure Level, under the flight path, for the effect geometrical spreading. The difference in distance from track to ground (r_2), with respect to the profile to ground distance (r_1) is corrected for using the relative height in Equation (6.2) and (6.3). Note that this procedure omits the effect of distance on the atmospheric absorption and is only used for illustrative purposes.

$$SPL(r_1) + 20\log_{10}(r_1) = SPL(r_2) + 20\log_{10}(r_2) \tag{6.2}$$

$$\frac{r_2}{r_1} = \varepsilon \tag{6.3}$$

Combining Equation (6.2) and (6.3), the geometrical spreading correction for the straight distance is calculated in Equation (6.4). Thus:

$$SPL(r_2) = SPL(r_1) - 20\log_{10}(\varepsilon) \tag{6.4}$$

The resulting geometrical spreading correction on the maximum A-weighted Sound Pressure Level under the flight path, where distance is equal to the height, is shown in Figure 6.12.

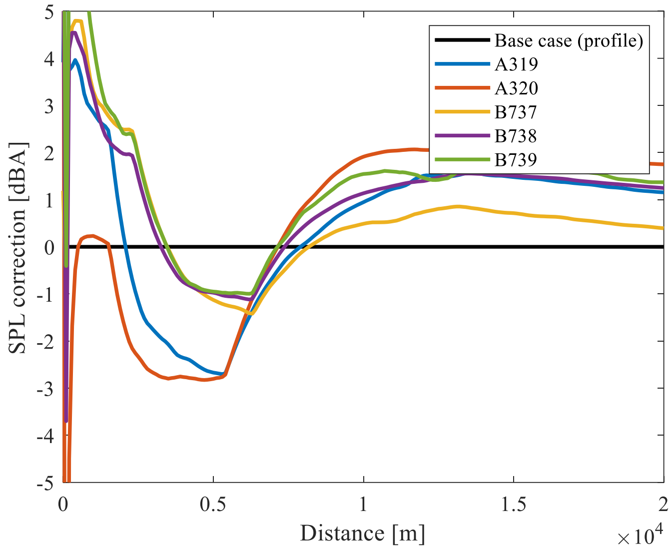

Figure 6.12. Sound Pressure Level correction under flight path as a result of difference in height

Figure 6.12 only accounts for the effect of geometrical spreading and is only valid under the flight path where the straight distance is determined by the height, so no lateral attenuation correction is needed. It can be seen that the under- and overestimation of the height can result in differences in noise levels up to several dB(A).

From these results, it becomes clear that the effect of the difference in height between the average track and the profile can already result in a several dB(A) correction to be applied to the noise levels under the flight path. This correction is the largest for the A319 and A320 at 2 to 5 km from the take-off, where an up to 3 dB correction is found.

To research this effect on the complete flight, the flights are also modelled by replacing the profile height for the real track height. The model then corrects for both the lateral attenuation and the noise level, resulting from the NPD-tables.

6.3.2. Track results

The tracks are for both runways modelled by using the individual ground track and replacing the profile height by the real track height. The SELs are calculated again for all 6 NMTs using the new input to the model. The result of the calculation with track heights on the individual SELs and type errors with respect to the NOMOS measurements are shown in Figure 6.13.

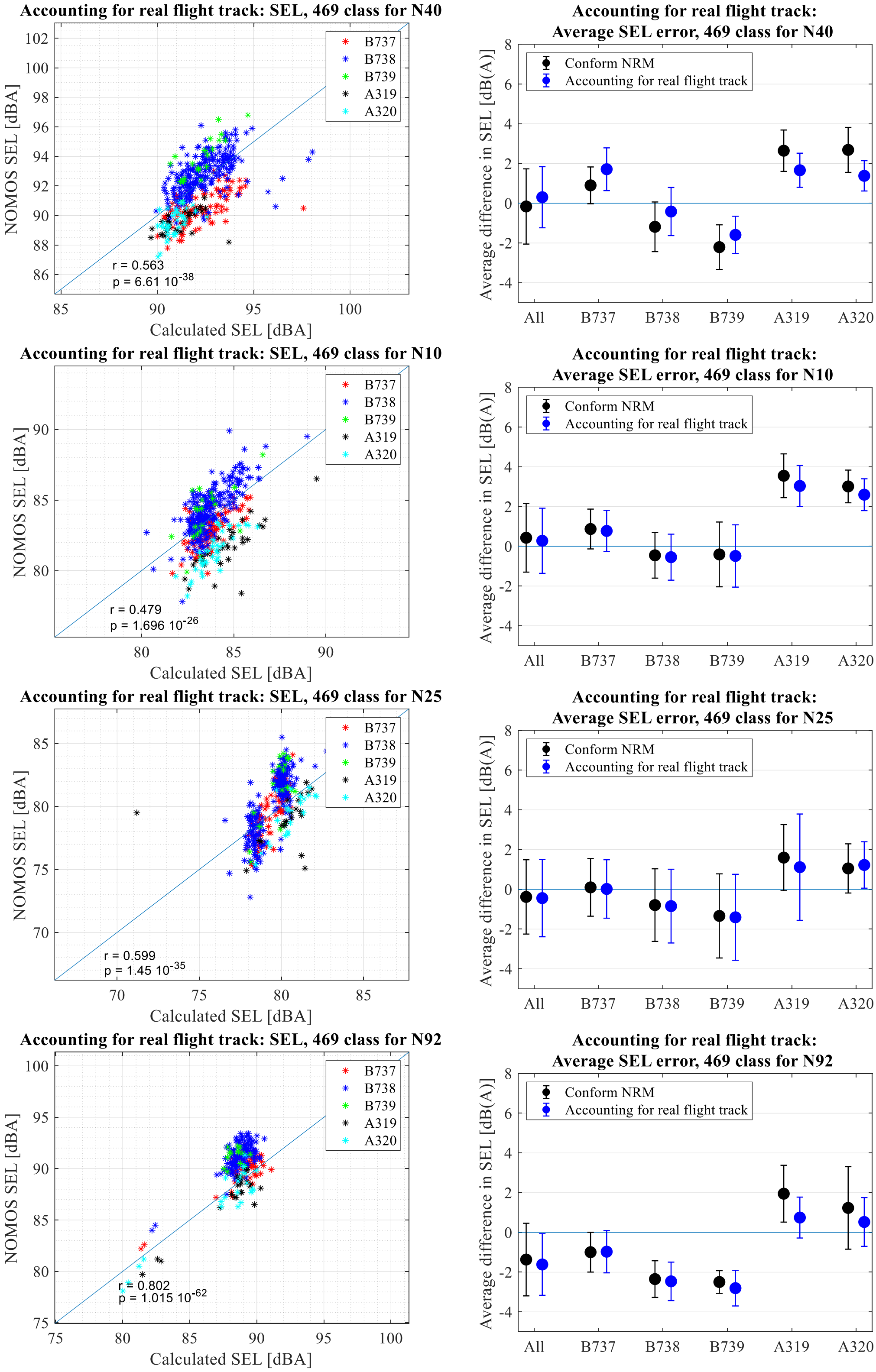

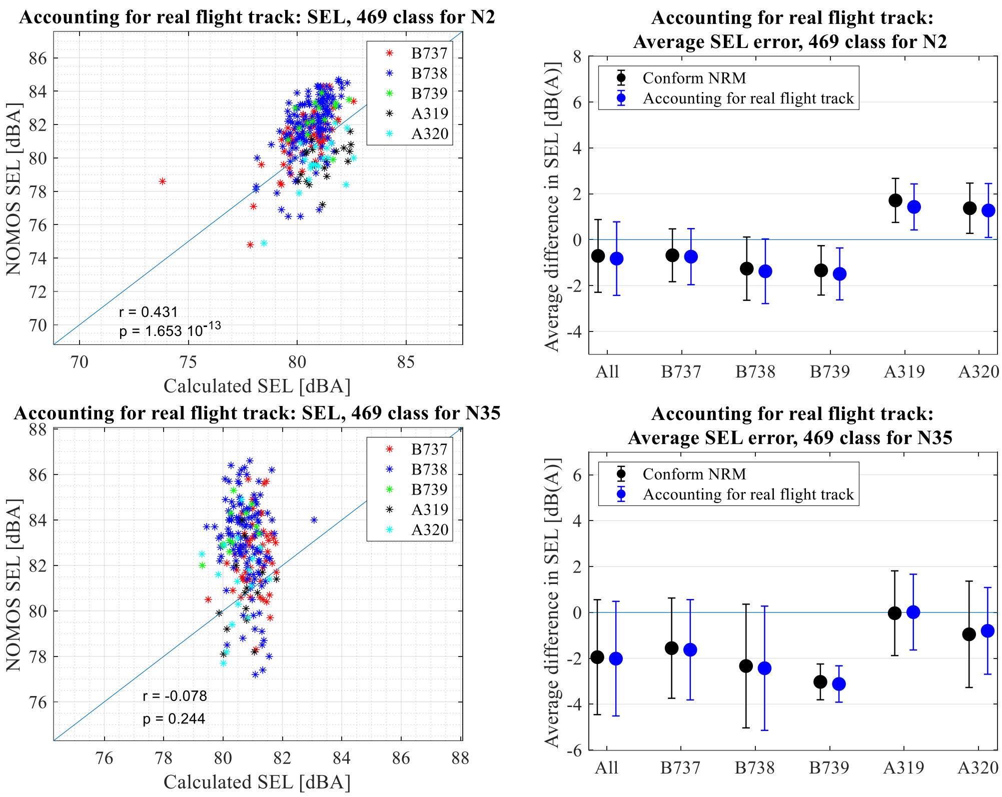

Figure 6.13. Accounting for real flight track: SEL calculations vs measurements for all 6 NMTs (left) and difference of average calculated SEL with respect to average measured SEL (right)

For most of the NMTs and types, there is no large improvement is found compared to the profile calculations. For these locations and aircraft, the track heights find a good match with the profile heights. However, the correlation of the data does improve for most of the NMTs compared to the theoretical profile calculations. In line with the results in Section 6.3.1, the largest impact can be found close to the runway at NMT 40, NMT 10 and NMT 92 for the Airbus A319 and A320. For these two aircraft types, the overestimation of the measured SELs by the model is now smaller compared to the profile calculation, resulting in calculations getting closer to the measurements. At NMT 40, located around 2-2.5 km from the runway, the calculated noise levels for all 3 Boeing aircraft increase, while for the A319 and A320 the calculated noise levels decrease, which is in line with the results found in Figure 6.12. The calculation with the track heights shows positive results for the B739 and B738, for which the average underestimation becomes smaller.

However, for the B737 at NMT40, a negative effect is found from the calculation with the track height compared to the profile height. This shows that only correcting for height is not enough to bring calculations closer to measurements. As the height profile is also linked to the thrust setting, more information about the thrust setting related to the height profiles is needed as well. This effect is analysed in the next part of this report.

6.4. Effect of thrust setting

This section analyses the effect of the thrust setting on the calculated noise levels. The real thrust setting is estimated from the flyover spectrogram using a frequency analysis for each aircraft type. The aircraft-specific thrust settings for NMT 40, 10, 25 and 2 are used as input to the model to add a thrust setting correction combined with the track heights.

6.4.1. Thrust setting estimation

The flight height is influenced by the engine thrust setting that is used by the pilot. As model input, the thrust settings are prescribed in the flight profiles, linked to the distance travelled. For the 4/3-class, a standard height profile and corresponding thrust setting for a 1500 ft NADP2 start, flight number 4690601, is shown in Figure 6.14.

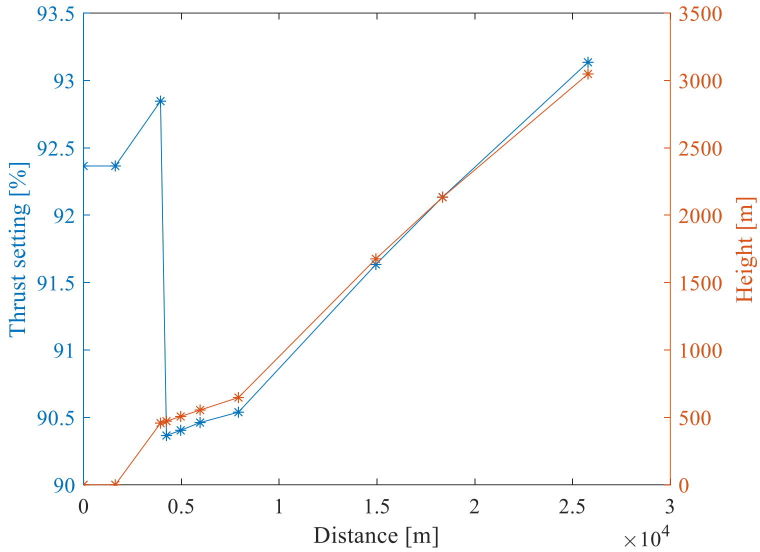

Figure 6.14. Theoretical height profile and thrust setting for flightnumber 4690601

However, since the real track height differs from the profile height, the real thrust settings deviate from prescribed thrust setting as well. This effect is analysed in this section, where a spectral analysis is used to derive the thrust setting from the dominant fan tone in the noise spectrum [15].

To do so, the mp3 audio files from NOMOS are used to acquire information about the noise spectrum. From this spectrum, the fan rpm is calculated using the undopplerized dominant fan tone. The dominant fan tone is derived by analysing spectrum for the complete flyover duration, as is shown in Figure 6.15.

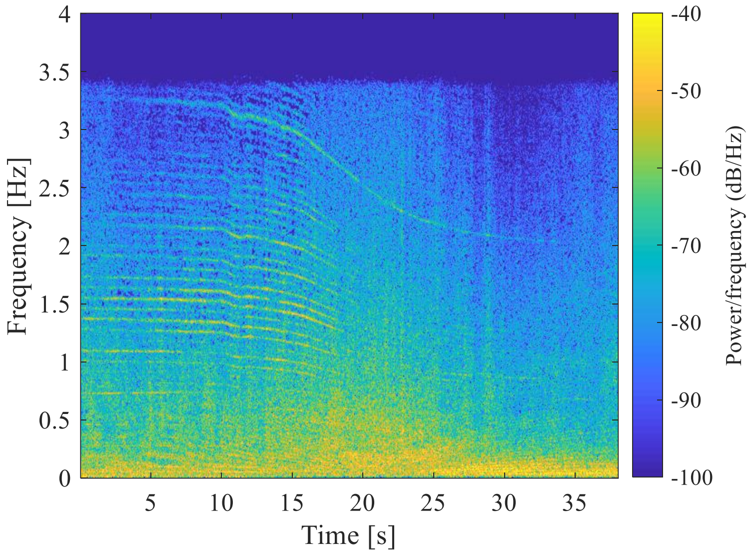

Figure 6.15. Spectrogram of an A320 flyover measured at NMT 40

The spectrogram in Figure 6.15 shows the flyover spectrum for an Airbus A320 take-off from runway 18L, passing by NOMOS NMT 40. The dominant tone, starting at around 3250 Hz for approach and decreasing to around 2000 for departure as a result of the doppler effect, is related to the fan. To derive the undopplerized tones (f) from this spectrogram, the frequencies in the spectrogram (f') are corrected for the relative flight speed. The relative flight speed follows from the change in straight distance (r) of the aircraft to the observer over time ($\frac{dr}{dt}$). Its fraction of the speed of sound (c) is the relative Mach number (M) and is used to calculate the frequency shift using Equation (6.5).

$$f = f'(1 + \frac{dr/dt}{c}) \tag{6.5}$$

The factor $\frac{dr/dt}{c}$ is negative for approach and positive for departure. For the exact overhead location, this factor is 0, indicating there is no shift in frequency. To correct for this shift, information about the flight path and location of the aircraft is needed. The spectrogram of the A320 shown in Figure 6.15 corresponds to the flight track for which the ground-track is shown in Figure 6.16.

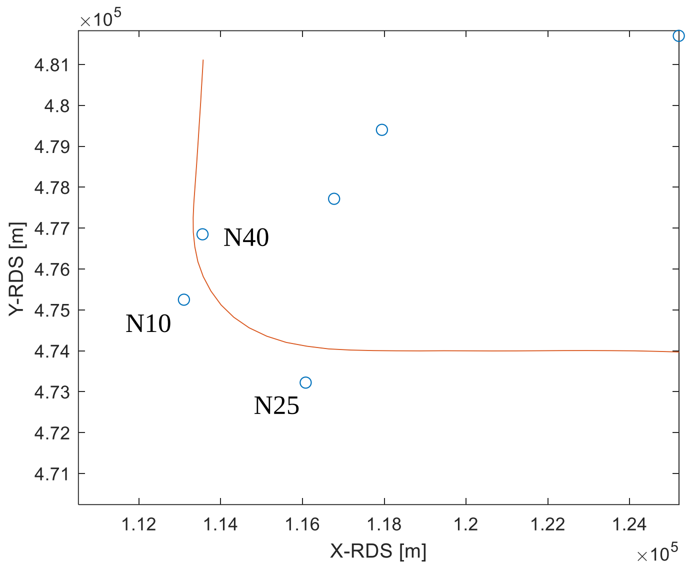

Figure 6.16. Reconstructed ground track A320 departure from 18L

From the ground track in Figure 6.16 and the corresponding height profile, the straight distance to each NMT can be calculated for the entire timespan of the flight. A 3D view, including the height, is shown in Figure 6.17.

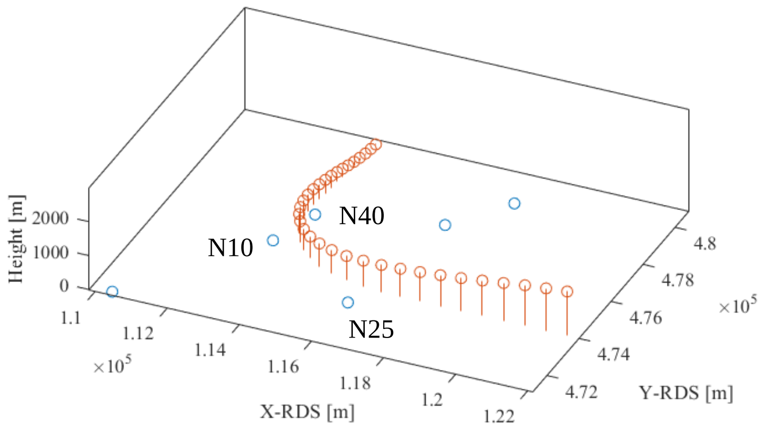

Figure 6.17. 3D reconstructed flight track A320 departure from 18L

Subsequently, the straight distance as a function of time ($r(t)$) from aircraft to NMT is calculated using the ground distance ($dX(t), dY(t)$) and distance in height ($dH(t)$) at each time (t), assuming the projection on the RDS coordinate frame does not lead to large errors [16].

$$r(t) = \sqrt{dX(t)^2 + dY(t)^2 + dH(t)^2} \tag{6.6}$$

Using Equation (6.6), the distance to the NMT is calculated for the emission-time of emission of the sound (t_e) and the reception-time at the NMT (t_r). The reception-time indicates the time at which the sound, travelling a distance r, is measured at the NMT as a result of the speed of sound. The latter is used to calculate the shift related to the measurements in reception-time. Both are shown in Figure 6.18.

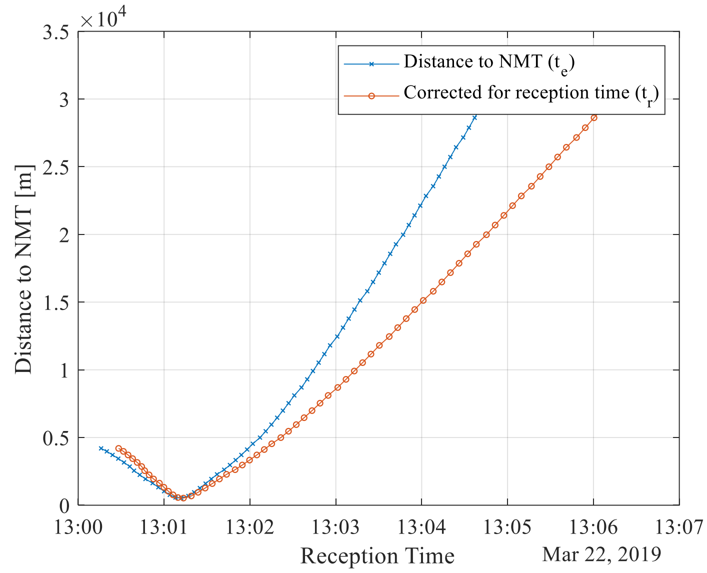

Figure 6.18. Straight distance to NMT over time and corrected for reception time

Using the change in distance to the NMT over time, the doppler shift is calculated using Equation (6.5). Before this factor is calculated, the number of datapoints is increased assuming a constant flight speed between subsequent data-points. After, the data is smoothed using a 5-point moving average filter. The factor $(1 + \frac{dr/dt}{c})$ that follows from the smoothed, refined data is shown in Figure 6.19.

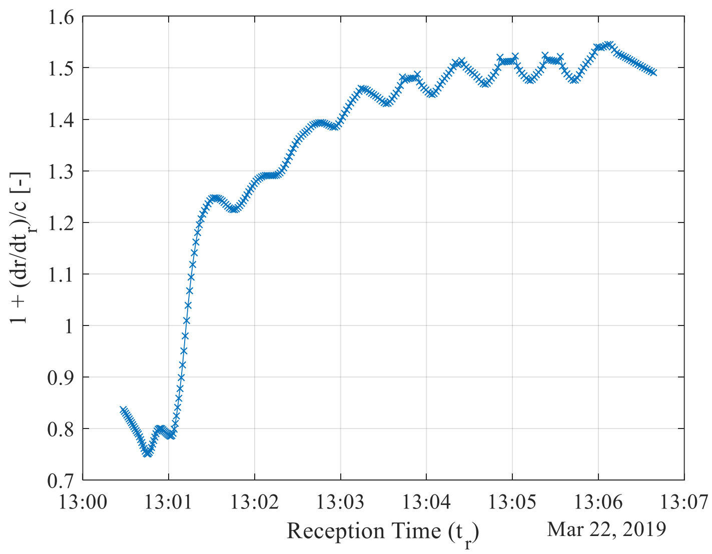

Figure 6.19. Doppler correction factor derived from distance to NMT

These factors are used to correct the frequencies as shown in the spectrogram of Figure 6.15. To do so, the track overhead time should be linked to the measurement overhead time as is determined from the audio file.

In a first step, the overhead time from the audio file is estimated by using the amplitude of the signal. At the overhead location, the signal amplitude is expected maximum, when neglecting directivity of the emitted noise, as the aircraft is closest to the receiver location. However, as there are strong pressure fluctuations and possible external effects influencing this pressure peak, a curve fit is applied to the data. This curve-fit follows the overall trend of the signal from which the estimated overhead location is found at 20 seconds.

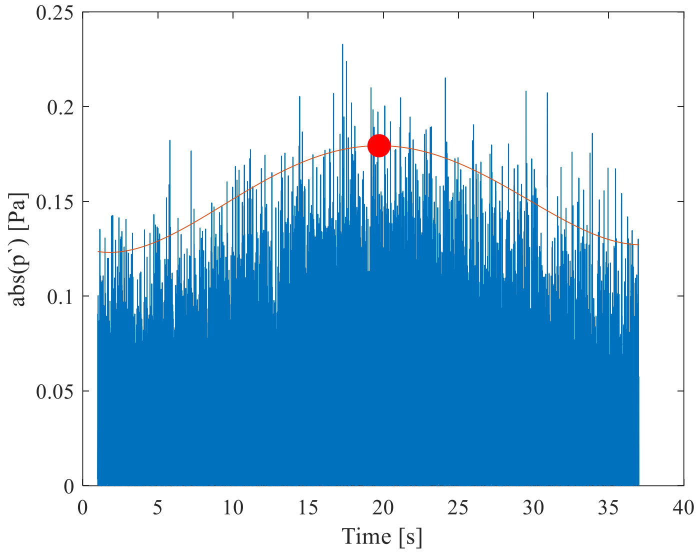

Figure 6.20. Absolute pressure fluctuation and curve-fit through peaks to estimate a maximum

The overhead time from the audio file found in Figure 6.20 is used as an initial guess to a first iteration to find the overhead time using the spectrogram. The overhead reception time of the spectrogram is located at the inflection point, i.e. the location where the second derivative equals zero. An initial overhead time guess, as follows from the pressure signal, is needed to fit a curve through the dominant fan tones. This time is matched to the overhead reception time from the flight-data to find the corresponding doppler correction factors. These time-specific correction factors are applied to all time-specific frequency spectra. To filter the data, only frequencies between feasible thresholds are considered. In this case, minima are set at 75% for the A319 and A320, 80% for the B737 and 85% for the B738 and B739 in order to get the best fitting results.

The (undopplerized) frequencies corresponding to the peaks for each time are plotted together with the original fan tones in Figure 6.21.

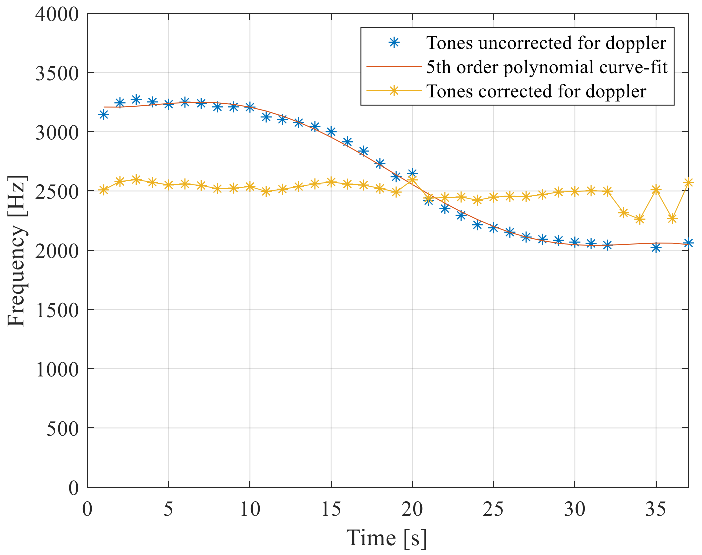

Figure 6.21. Strongest undopplerized frequencies for each timeset with the corresponding original tones

Based on this curve-fit in Figure 6.21, the overhead location is found by locating minimum of the first derivative (df/dt), i.e. where the inflection point is located. The first derivative of this curve-fit with respect to time (df/dt), is shown in Figure 6.22.

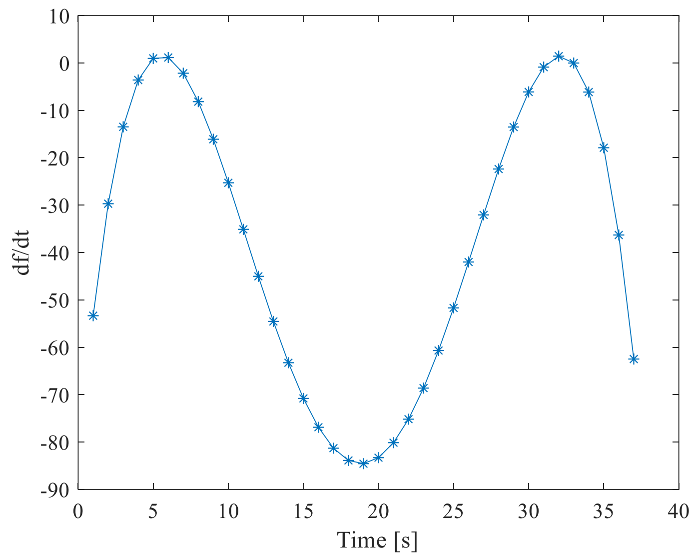

Figure 6.22. First derivative of curve fit through fan tones

From Figure 6.22, the minimum, $\frac{d^2f}{dt^2} = 0$, is found at a time of 19 seconds. This value is used for the next iteration, where the time of 19 seconds is used as match for track overhead time and audio file overhead time. Resulting in a new curve-fit of the fan tones as shown together with doppler-corrected fan tones and the spectrogram in Figure 6.23.

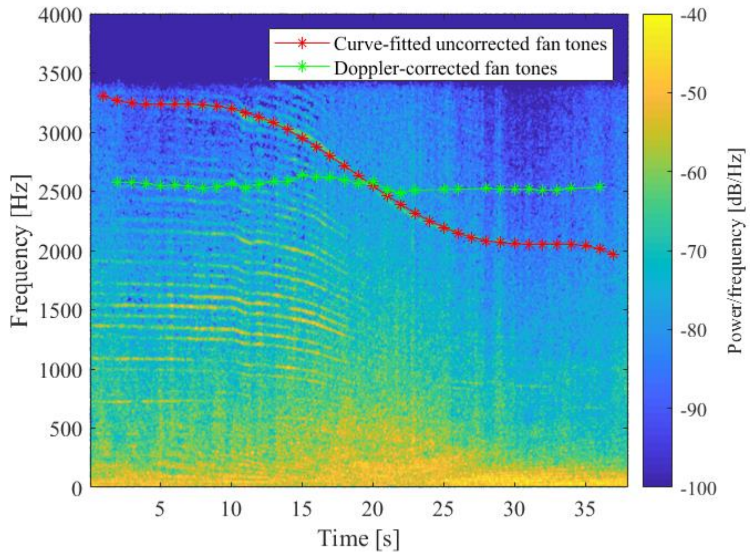

Figure 6.23. Spectrogram indicating the derived original fan tones the corrected fan tones

The data-gaps in the corrected fan tones belong to the outliers that have been removed in the process. These outliers are for example related to external noise leading to stronger peaks at other frequencies, or lower harmonics of the single fan-blade frequency. The data without outliers is used to calculate the mean of the fan tones for this flyover. The undopplerized spectrogram of the analysed signal corresponding to the doppler-corrected fan tones in Figure 6.23, is shown in Figure 6.24.

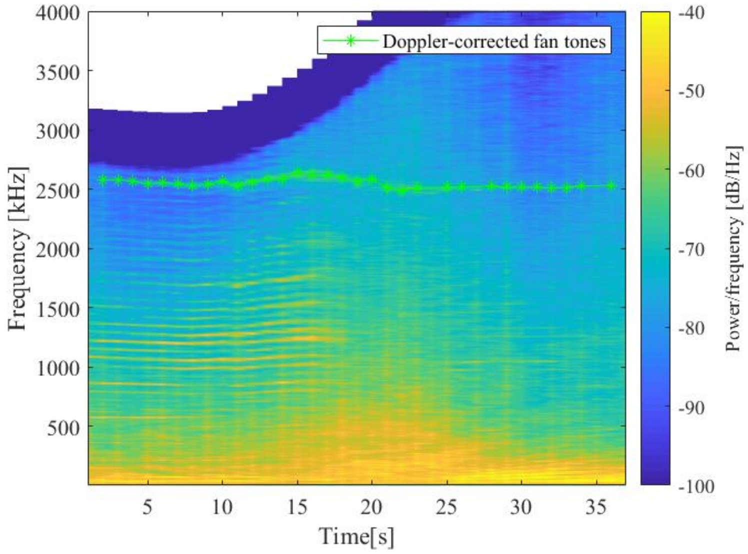

Figure 6.24. Undopplerized spectrogram with the derived fan tones

To convert the fan tone to an engine rotational speed, the number of fan blades is required. The engine fan tone is equal to the Blade Passing Frequency (BPF), in rpm, which is related to the engine rotational speed (n), in rpm, and the number of blades (B) following Equation (6.7).

$$BPF = f = B\frac{n}{60} \tag{6.7}$$

The A319s and A320s as analysed in this section all make use of the CFM56-5B engine by CFM International. The CFM56-5B engine fan consists of 36 fan blades and has a maximum rotational speed, 104% N1, of 5200 rpm [17].

For the fan tones shown in Figure 6.24, the mean rpm is calculated using Equation (6.7) and the engine specifications. The mean, undopplerized fan tone is for this flyover, at NMT 40, equal to 2550 Hz. This corresponds to a fan rotational speed of 4250 rpm which is 85.0% of the specified N1.

This process is strongly dependent on the overhead time guess, where a small under- or overestimation of the overhead time can lead to a several percent deviation in thrust setting. For this reason, all further results are checked for validity and if needed adjusted manually.

6.4.2. Thrust results

The same process is repeated for a total of 200 flights in 2019, as the original audio files of the 2018 flights were not available anymore. The audio files are taken from NMT 40, 10 and 25 (18L) and NMT 2 (36C) to analyse multiple locations along the flight path and exclude runway-specific effects. NMT 35 and 92 did not provide (reliable) audio files and are for this reason not included in the research. For all 200 flights, the airlines that operate the aircraft are the same as the flights that are used in this research to exclude airline-specific procedure effects and get the best representation possible to the 2018 dataset. The total number of 200 flights is equally divided over the aircraft types and the 4 NMTs resulting in 10 measurements per aircraft type per NMT.

All three of the analysed Boeing aircraft, by KLM and Transavia, use the CFM56-7B engine, with a fan consisting of 24 blades and a maximum rotational speed, 104% N1, of 5382 rpm [18]. The Airbus aircraft both use the CFM-56-5B engine, with a 36 bladed fan disk and a maximum rotational speed of 5200 rpm [19].

An overview of the derived thrust settings for NMT40 is shown in Figure 6.25 which illustrates the results in a boxplot form.

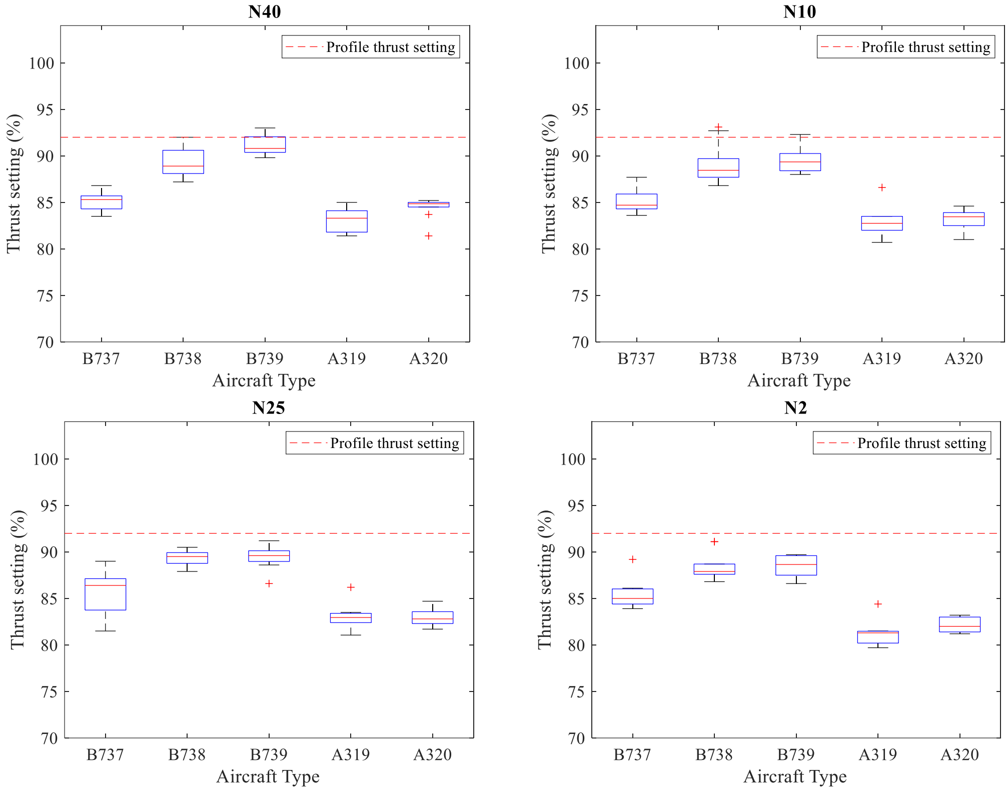

Figure 6.25. Derived thrust settings at 4 NMTs

The results show that for all aircraft types and all NMTs, the overall derived engine setting is lower than the used engine setting in the theoretical profile calculations. Next to this, it shows that there is a clear difference in engine setting for each aircraft type within this class which is not included in the theoretical calculations as a result of the classification.

By extending this research to the other NMTs, it becomes clear that the same trend is found for all NMTs. The average rpm per type per NMT as a result of these 200 flights are shown in Table 6.1.

Table 6.1. Average thrust settings at 4 NMTs

	B737	**B738**	**B739**	**A319**	**A320**
NMT 40 [%]	85.2	89.4	91.2	83.1	84.4
NMT 10 [%]	85.3	89.2	89.5	82.9	83.2
NMT 25 [%]	85.7	89.3	89.4	83.1	83.0
NMT 2 [%]	85.4	88.4	88.4	81.3	82.1

All of the average thrust settings are lower than the thrust settings that are used in the profile as shown in Figure 6.14. For this reason, noise levels calculated from the profiles are, as a result of the thrust setting, higher than the levels that are calculated when correcting for the derived thrust setting for all aircraft types for the analysed NMTs.

The noise levels are re-calculated using the model by replacing the theoretical profile thrust by the derived thrust setting for each aircraft type. Again, the profile heights are replaced by the real track heights to correct for track height and thrust setting. The results of the calculations are compared to the measured noise levels and shown in Figure 6.26.

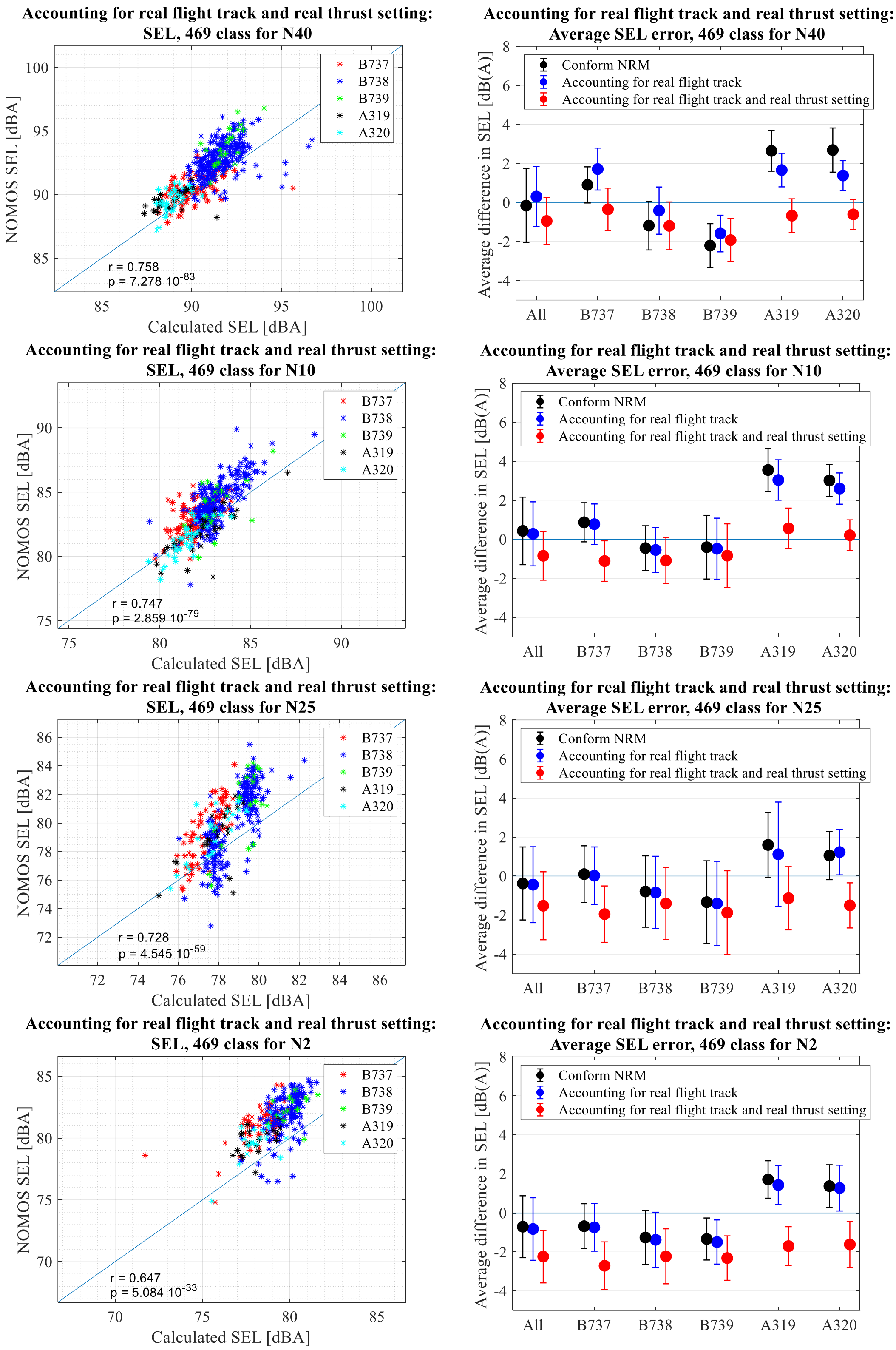

Figure 6.26. Accounting for real flight track and thrust setting: SEL calculations vs measurements for all 6 NMTs (left) and difference of average calculated SEL with respect to average measured SEL (right)

Figure 6.26 shows that in all situations, the correlation coefficient improves again. It can be seen that for all NMTs and aircraft types, the lower thrust setting results as expected in lower calculated noise levels compared to the track correction only. For most of the results, except for the Airbus A319 and A320 at NMT10, this now results in lower average calculated noise levels compared to the average measured noise levels. For NMT 25 and NMT 2, these errors are larger than the errors found for NMT 40 and NMT 10.

The best explanation for these larger errors for NMT 25 and NMT 2 is the fact that both NMTs are located in the outside the curved flight path. Because of this, the bank angle of the aircraft leads to higher noise emission in the direction of the NMTs. This results in higher measured noise levels than would be measured for a straight flight path as is the case for NMT 40 and NMT 10. It is recommended to test this hypothesis for further improvement of the model.

6.5. Explanations for aircraft specific differences

Differences in thrust setting and height profile can be explained based on two aircraft specific characteristics that play a role in the produced thrust and climb performance. First, the classification represents all aircraft in the 469 class by a B737-300 HWFAP using the older CFM56-3B engines with a maximum take-off thrust of 98300 N. The Airbus and Boeing aircraft used in this research use the newer CFM56-5B and CFM-7B engines respectively. The CFM56-7B24, used by the B737(-700), is capable of delivering 107650 N thrust during take-off, yielding a more than 9.5% increase in thrust compared to the CFM56-3B. The B738 and B739 use the CFM56-7B27 engines, delivering 121440 N of thrust, yielding an increase of 12.8% compared to the B24 and an increase of 23.5% compared to the CFM56-3B [20]. The CFM56-5B, used by the A319 and A320, has a maximum take-off thrust of up to 120100 N. This is an increase of 11.7% compared to the CFM56-7B24 and a 22.1% compared to the CFM56-3B [21]. The higher maximum thrust settings partly explain the lower thrust setting that is found from the thrust estimations compared to the theoretical thrust setting set for the class, assuming equal take-off weights.

Next to the thrust setting, the weight of the aircraft also influences the flight performance of the aircraft. The maximum weight that is used in the classification, linked to the highest distance class, is 58700 kg. This is 93.4% of the Maximum Take-Off Weight ($MTOW$) of the B737-300, being 62820 kg. However, the aircraft that are used in this research, represented by the B737-300, all have $MTOW$s higher than this. For example, the B737-700, which has with 65300 kg the lowest $MTOW$ of the used aircraft, is already 4% heavier than its B737-300 counterpart.

To capture both the Maximum Take-off Thrust ($MTOT$) for 2 engines, in Newton, and Maximum Take-off Weight ($MTOW$), in kg, the Thrust-to-Weight ratio (TW) is calculated (Equation (6.8)) [22].

$$TW = \frac{MTOT}{9.81 * MTOW} \tag{6.8}$$

An overview of the specifications per aircraft type is shown in Table 6.2.

Table 6.2. Aircraft specifications compared to representative aircraft (B737-300)

Aircraft Type	MTOT [N] (2 engines)	MTOW [kg]	TW [-]	Compared to 737-300
B737-300 (CFM56-3B)	196600	62820	0.320	-
B737-700 (CFM56-7B24)	215120	65300	0.336	+ 5%
B737-800 (CFM56-7B27)	242880	73700	0.336	+ 5%
B737-900 (CFM56-7B27)	242880	76900	0.322	+ 0.625%
A319 (CFM56-5B4)	240200	75500	0.324	+ 1.25%
A320 (CFM56-5B4)	240200	78000	0.314	- 2%

Even though there are large differences in MTOW and MTOT for all aircraft, the TW shows only a maximum of 5% difference compared to the representative aircraft. However, when assuming the same real take-off weight for all aircraft, as given in the profile, a lower thrust setting is required for all used aircraft to deliver the required thrust, which is in line with the results found. To explain the aircraft specific differences in more detail, FDR data and take-off weights are needed.

7

Conclusion and recommendations

The modelling and calculation of noise events already shows differences on a very detailed scale. Where noise models assume general circumstances, the measured noise events are influences by the imposed noise level fluctuations, resulting in unexpected deviations from an 'ideal' shape. This becomes clear when the NRM model is used for single event comparison with measurements by modelling a complete noise event time-series.

By looking at multiple events within the same class, and comparing the modelled noise levels with measurements, it is found that the model shows consistent errors for the individual types included in the class. From these type-specific errors, it can already be concluded that the classification as is does not represent all individual aircraft types equally well. The consistent errors indicate that the individual aircraft types show in practice different behaviour than in theory.

These differences are explained based on two input parameters: flight height and thrust setting. Analysis on the real flight heights compared to the standard theoretical input profiles showed that the real flight heights are not represented correctly by the theoretical profiles. First of all, the A319 and A320 are in practice not following the 1000ft NADP2 procedure, as is originally stated, but follow the 1500ft NADP2 like the Boeing aircraft. Furthermore, significant differences in height are found for the early stages of the take-off, where the average track height deviates from the ideal profile height for all aircraft types. When correcting for both effects, the largest improvements can be found closest to the runway for the Airbus aircraft. However, for the B737 this has a negative effect on the results, leading to a larger deviation from the measurements. This shows that there is another effect that should be taken into account, being the thrust setting. For the model, the thrust setting is prescribed linked to the theoretical height profile, in line with the equations of motion. In reality, as the real height differs, deviations in thrust setting are expected as well. Using a frequency analysis, the fan tones and corresponding engine rotational speeds are derived. For all aircraft, this results in lower thrust setting than theoretically used as input to the model. Next to this, a consistent difference in thrust setting is found between all individual aircraft types. This again confirms that the classification as is, using the same thrust setting for each aircraft type, does not align with practice.

When correcting for the found thrust setting for each aircraft type specifically, the correlation of the measurements and calculations increases significantly. However, for most of the situations, this on average results in an underestimation of the measured noise levels by the model calculations, where the largest underestimations are found for curved flight paths. Because of this, the effect of the curved flight path on the bank angle and resulting noise levels is recommended for further research.

A partial explanation for the remaining differences can be found in the aircraft specific characteristics. All individual aircraft types that are used in this class have different characteristics in terms of Maximum Take-Off Weight and Maximum Take-Off Thrust. Where the difference in MTOW is a result of the difference in size and manufacturer, the MTOT follows from the used engine type. The noise data used in the model comes from the representative, but older, B733 aircraft with the old CFM56-3B engines. The newer aircraft types that are used in this analysis all have a higher MTOW than the B733 and use the newer CFM56-7B (Boeing) and CFM56-5B (Airbus) engine types. This results in higher MTOTs and higher thrust found for the same engine setting. It should however be noted that all resulting Thrust-to-Weight ratios are comparable to the B733, with an up to a 5% difference in favour of the newer Boeing aircraft.

Recommendations

The following recommendations contribute to model improvement and improvement of the used information systems. The model improvements aim at bringing the model closer to reality, while the other recommendations aim at improving the workflow of acquiring and processing the data.

Class data improvement

As shown in this research, the theoretical input data can differ significantly from the real flight. It is recommended to regularly update this flight data as airline specific procedures and new aircraft types result in deviations of flight height profile and thrust setting related to this. Updating this data brings the model input closer to reality and allows for a better comparison of calculations with measurements. Furthermore, it is recommended to revise the classification by a redistribution into smaller classes represented by aircraft types that are present at the airport, ideally including engine type. As the analysed class represents approximately 50% of all flights at Schiphol Airport, individual type-specific errors will have a large impact on the total calculated noise exposure.

Further comparison with reality

To explain how aircraft type characteristics work through to the differences in calculated and measured noise levels, more information is needed about the real thrust settings and take-off weights. It is recommended to have this information available when comparing noise models to measurements to reduce input-related errors. Lastly, the model has a limited use as weather condition corrections are not available. It is recommended to add these corrections to allow for a larger dataset to be analysed.

Flyover radar data sampling rate

To get a more accurate position of the aircraft during flyover, radar data sampling rate should be improved. At this moment, the position is determined every 4 seconds. This is good enough for flight path reconstruction using linear interpolation assuming constant speed, but loses information about the location and speed in between the measurements. This leads to uncertainty in exact flyover location and speed, used for the calculation of the fan tones.

NOMOS measurement conversion to mp3

With the conversion to mp3 audio files, at 8 kHz, a lot of data is lost about the higher frequency spectrum. This frequency spectrum contains information about engine parts rotating at a higher rpm, like the High-Pressure Compressor and High-Pressure Turbine. Next to this, comparison with the NOMOS measurements, using raw data at 48 kHz, showed that the resampling to mp3 results in a more than 10 dB(A) lower reconstructed A-weighted Sound Pressure Level at NMT40 for the complete event.

Central flight information system

Schiphol’s central flight information system (CISS) is not linked to the ANOMS database used for NOMOS measurements. As a result, each flight is assigned an ID by both NOMOS and LVNL which are different and not communicated. Because of this, the linking of the noise events to LVNL flight data is necessary even though NOMOS already has flight information available for each event.

API for ANOMS database

The ANOMS database that is used for accessing NOMOS measurements only allows for manual retrieval of data. Introducing an API that can be linked to the flight data could significantly reduce the workload that is needed. Furthermore, it would allow for continuous improvement of the model by year-round direct comparison of calculations with measurements.

NOMOS aircraft detection system

As is seen from NMT35, NMTs cannot distinguish aircraft noise from background noise. While the aircraft is within a feasible area from the NMT, all noise is captured independent of the source. As a result, measurements include both aircraft noise and background noise in the total Sound Exposure Levels resulting in offsets between measurements and calculations at locations where background noise is dominantly present. If the NMTs are able to distinguish aircraft noise from background noise, for example using noise characteristics, the system can exclude other noise sources, leading to better measurements of aircraft-related noise.

Bibliography

1. Statistiek, C.B.v.d., *Bijna 80 miljoen passagiers op Nederlandse Luchthavens*. 2018.
2. van Veldhoven - van der Meer, S., *Actieplan Schiphol 2018-2023*, M.v.I.e. Milieu, Editor. 2018: Den Haag.
3. Adviescommissie Geluidhinder door Vleigtuigen, *Rapport Geluidhinder door Vliegtuigen*. 1967.
4. Wal, H.M.M.v.d., P. Vogel, and F.J.M. Wubben, *Voorschrift voor de berekening van de Lden en Lnight geluidbelasting in dB(A) ten gevolge van vliegverkeer van en naar de luchthaven Schiphol*. 2001, National Aerospace Laboratory NLR.
5. Heppe, G.J.T., *Appendices van de voorschriften voor de berekening van de geluidsbelasting in Lden en Lnight voor Schiphol*. 2014, National Aerospace Laboratory.
6. Eurocontrol. *ATM surveillance tracker and server*. 2019 [cited 2019 03-06-2019]; Available from: https://www.eurocontrol.int/artas.
7. Schiphol, L. *Schiphol Amsterdam Airport NOMOS Online*. [cited 2019 27/05/2019]; Available from: http://noiselab.casper.aero/ams/#page=home.
8. International Civil Aviation Organisation, *Environmental Protection - Aircraft Noise.* 2008. **1**.
9. Engines, M.A. *Noise Reduction by New Engine Concepts*. in *ICANA 2013*. 2013. Frankfurt.
10. Simons, D.G., *Introduction to Aircraft Noise.* 2017.
11. Harris, C.M., *Absorption of sound in air versus humidity and temperature.* The Journal of the Acoustical Society of America, 1966. **40**(1): p. 148-159.
12. Oliveira, A.F.G.P.d., *The effect of wind and turbulence on sound propagation in the atmosphere*, in *Engenharia Aeroespacial*. 2012, Universidade Técnica de Lisboa.
13. Olshausen, B.A., *Aliasing*. 2000, Redwood Center for Theoretical Neuroscience.
14. Plc, S., *Window Types: Hanning, Flattop, Uniform, Tukey, and Exponential*. 2017: Online.
15. Merino-Martinez, R., et al., *Improving Aircraft Noise Predictions Considering Fan Rotational Speed*. 2018. 1-11.
16. Wal, H.M.M.v.d., P. Vogel, and F.J.M. Wubben, *Voorschrift voor de berekening van de Lden en Lnight geluidbelasting in dB(A) ten gevolge van vliegverkeer van en naar de luchthaven Schiphol*. 2001, National Aerospace Laboratory NLR.
17. Agency, E.A.S., *Type-Certificate Data Sheet No. E.003 for CFM56-5B and CFM56-5C series engines*. 2017: Paris.
18. Agency, E.A.S., *Type-Certificate Data Sheet No. E.004 for CFM56-7B series engines*. 2012.
19. Engines, C.A., *EasyJet orders additional CFM56-5B engines*. 2014: Westchester.
20. Engines, S.A. *CFM56-7B: the exclusive Boeing 737NG engine*. Available from: https://www.safran-aircraft-engines.com/commercial-engines/single-aisle-commercial-jets/cfm56/cfm56-7b.
21. Engines, S.A. *The CFM56-5B PIP: the engine of choice for the A320ceo family*. Available from: https://www.safran-aircraft-engines.com/commercial-engines/single-aisle-commercial-jets/cfm56/cfm56-5b.
22. Administration, N.A.a.S., *Thrust to Weight Ratio*. Glenn Research Center.